NLO twist-3 contributions to $B \to \pi$ form factors in k_T factorization

Shan Cheng,[1] Ying-Ying Fan,[1] Xin Yu,[2] Cai-Dian Lü,[2,*] and Zhen-Jun Xiao[1,3,†]

[1]*Department of Physics and Institute of Theoretical Physics, Nanjing Normal University, Nanjing, Jiangsu 210023, People's Republic of China*

[2]*Institute of High Energy Physics and Theoretical Physics Center for Science Facilities, Chinese Academy of Sciences, Beijing 100049, People's Republic of China*

[3]*Jiangsu Key Laboratory for Numerical Simulation of Large Scale Complex Systems, Nanjing Normal University, Nanjing 210023, People's Republic of China*

(Received 26 February 2014; published 5 May 2014)

In this paper, we calculate the next-to-leading-order (NLO) twist-3 contribution to the form factors of $B \to \pi$ transitions by employing the k_T factorization theorem. All the infrared divergences regulated by the logarithms $\ln(k_{iT}^2)$ cancel between those from the quark diagrams and from the effective diagrams for the initial B meson wave function and the final pion meson wave function. An infrared finite NLO hard kernel is, therefore, obtained, which confirms the application of the k_T factorization theorem to the B meson semileptonic decays at the twist-3 level. From our analytical and numerical evaluations, we find that the NLO twist-3 contributions to the form factors $f^{+,0}(q^2)$ of the $B \to \pi$ transition are similar in size but have an opposite sign with the NLO twist-2 contribution, which leads to a large cancellation between these two NLO parts. For the case of $f^+(0)$, for example, the 24% NLO twist-2 enhancement to the full LO prediction is largely canceled by the negative (about -17%) NLO twist-3 contribution, leaving a small and stable 7% enhancement to the full LO prediction in the whole range of $0 \le q^2 \le 12\ \mathrm{GeV}^2$. At the full NLO level, the perturbative QCD prediction is $F^{B\to\pi}(0) = 0.269^{+0.054}_{-0.050}$. We also study the possible effects on the perturbative QCD predictions when different sets of the B meson and pion distribution amplitudes are used in the numerical evaluation.

DOI: 10.1103/PhysRevD.89.094004 PACS numbers: 12.38.Bx, 12.38.Cy, 12.39.St, 13.20.He

I. INTRODUCTION

Without end-point singularity, the k_T factorization theorem [1–3] is a better tool to deal with the small x physics when comparing with other factorization approaches [4–8]. Based on the k_T factorization theorem, the perturbative QCD (pQCD) factorization approach [9–12] is a successful factorization approach to handle the heavy to light exclusive decay processes. As an effective factorization theorem, the k_T factorization should be valid at every order expanded by strong coupling $O(\alpha_s^n)$, where n is the power of the expansion.

Recently, the next-to-leading-order (NLO) twist-2 (the leading twist) contributions to the form factors for the $\pi\gamma^\star \to \gamma$, $\pi\gamma^\star \to \pi$, and $B \to \pi$ transitions have been evaluated [13–15] by employing the k_T factorization theorem [1–3], and an infrared finite k_T-dependent hard kernel was obtained at the NLO level for each considered process. It is worth of mentioning that new progress about the pion form factor in the $\pi\gamma^* \to \gamma$ scattering has been made in Ref. [16] very recently, where the authors made a joint resummation for the pion wave function and the pion transition form factor and proved that the k_T factorization is scheme independent. These NLO contributions could produce sizable effects to the LO hard kernels. For example, the NLO twist-2 contribution to the form factor $F_0^{B\to\pi}(0)$ for the $B \to \pi$ transition can provide an $\sim$30% enhancement to the corresponding full LO form factor [15]. In a recent paper [17], we calculated the NLO twist-3 contribution to the pion electromagnetic form factor $F_{\pi\gamma}(Q^2)$ in the $\pi\gamma^\star \to \pi$ process by employing the k_T factorization theorem and found infrared finite NLO twist-3 corrections to the full LO hard kernels [17].

In this paper, following the same procedure of Ref. [15], we will calculate the NLO twist-3 contribution to the form factor of the $B \to \pi$ transition, which is the only missing piece at the NLO level. The light partons are also considered to be off shell by k_T^2 in both the QCD quark diagrams and effective diagrams for hadron wave functions. The radiation gluon from the massive b quark generates the soft divergence only. Such soft divergence can be regulated either by the virtuality of internal particles or by the virtuality the k_T^2 of other light partons, to which the emission gluons were attached. So we can replace the off-shell scale k_T^2 for the light parton by m_g for the massive b quark safely to regulate the IR divergences from the massive b quark line, where m_g means the mass of the gluon radiated from the b quark. That means, the b quark remains on shell in the framework.

We will prove that the IR divergences in the NLO QCD quark diagrams could be canceled by those in the effective

*lucd@ihep.ac.cn
†xiaozhenjun@njnu.edu.cn

diagrams, i.e., the convolution of the $O(\alpha_s)B$ meson and π meson wave functions with the LO hard kernel. The IR finiteness and k_T-dependent NLO hard kernel were also derived at the twist-3 level for the $B \to \pi$ transition form factor, which confirms the application of the k_T factorization theorem to the B meson semileptonic decays at both the twist-2 and twist-3 levels.

In our calculation for the NLO twist-3 contribution, resummation technology [18,19] is applied to deal with the large double logarithms $\alpha_s \ln^2 k_T$ and $\alpha_s \ln^2 x_i$, where x_i is the parton momentum fraction of the antiquark in the meson wave functions. With appropriate choices of μ and μ_f, say, being lower than the B meson mass, the NLO corrections are under control. From the numerical evaluations, we find that the NLO correction at the twist-3 contribution is about -17% of the LO part, while the NLO twist-2 contribution can provide a 24% enhancement to the LO one. This means that the NLO twist-2 contribution to the form factor $F^{B\to\pi}(0)$ is largely canceled by the NLO twist-3 one and leaves a net small correction to the full LO form factor, around or less than a 7% enhancement.

The paper is organized as follows. In Sec. II, we give a brief introduction of the calculations of the LO diagrams relevant with the form factor of the $B \to \pi$ transition. In Sec. III, we calculate the NLO twist-3 contribution to the $B \to \pi$ form factor. The relevant $O(\alpha_s^2)$ QCD quark diagrams are calculated analytically, and the convolutions of the $O(\alpha_s)$ wave functions and $O(\alpha_s)$ hard kernel are made in the same way as those for the evaluation of the NLO twist-2 contribution. Finally, we extract out the expression of the factor $F^{B\to\pi}_{\text{NLO-T3}}(x_i, \mu, \mu_f, \eta)$, which describes the NLO twist-3 contribution to the form factor $F^{B\to\pi}(x_i, \mu, \mu_f, \eta)$. In Sec. IV, we calculate and present the numerical results for the relevant form factors and examine the q^2 dependence of $F^+(q^2)$ and $F^0(q^2)$ at the LO and NLO levels, respectively. A short summary is given in the final section.

II. LO ANALYSIS

By employing the k_T factorization theorem, the LO twist-2 and twist-3 contributions to the form factor of $B \to \pi$ transition were calculated many years ago [9–12]. For the sake of the readers, here we present the expressions of the leading-order hard kernels directly.

The $B \to \pi$ transition form factors are defined via the matrix element

$$\langle \pi(p_2)|\bar{u}\gamma^\mu b|B(p_1)\rangle = f^+(q^2)(p_1^\mu + p_2^\mu) + [f^0(q^2) - f^+(q^2)]\frac{m_B^2 - m_\pi^2}{q^2} q^\mu, \quad (1)$$

where $m_B(m_\pi)$ is the $B(\pi)$ meson mass, and $q = p_1 - p_2$ is the transfer momentum. The momentum $p_1(p_2)$ is chosen as $p_1 = p_1^+(1, 1, \mathbf{0}_T)[p_2 = (0, p_2^-, \mathbf{0}_T)]$ with the component $p_1^+ = m_B/\sqrt{2}$ and $p_2^- = \eta m_B/\sqrt{2}$. Here the parameter $\eta = 1 - q^2/m_B^2$ represents the energy fraction carried by the pion meson and $\eta \sim O(1)$ when in the large recoil region of the pion. According to the k_T factorization, the antiquark $\bar{q}$ carries momentum $k_1 = (x_1 p_1^+, 0, \mathbf{k}_{1T})$ in the B meson and $k_2 = (0, x_2 p_2^-, \mathbf{k}_{2T})$ in the pion meson as labeled in Fig. 1, with x_1 and x_2 being the momentum fractions. The following hierarchy is postulated in the small-x region:

$$m_B^2 \gg x_2 m_B^2 \gg x_1 m_B^2 \gg x_1 x_2 m_B^2, k_{1T}^2, k_{2T}^2, \quad (2)$$

which is roughly consistent with the order of magnitude: $x_1 \sim 0.1$, $x_2 \sim 0.3$, $m_B \sim 5$ GeV, and $k_T \lesssim 1$ GeV [15].

The LO hard kernels are obtained after sandwiching Fig. 1 with the B meson and the pion meson wave functions [9,10,20]

$$\Phi_B(x_1, p_1) = \frac{1}{2\sqrt{N_c}}(\not{p}_1 + m_B)\gamma_5 \times \left[\not{n}_+ \phi_B^+(x_1) + \left(\not{n}_- - k_1^+ \gamma_\perp^\nu \frac{\partial}{\partial \mathbf{k}_{1T}^\nu}\right)\phi_B^-(x_1)\right], \quad (3)$$

$$\Phi_\pi^{T2}(x_2, p_2) = \frac{1}{\sqrt{2N_c}}\gamma_5 \not{p}_2 \phi_\pi^A(x_2), \quad (4)$$

$$\Phi_\pi^{T3}(x_2, p_2) = \frac{1}{\sqrt{2N_c}} m_0 \gamma_5 [\phi_\pi^P(x_2) - (\not{n}_- \not{n}_+ - 1)\phi_\pi^T(x_2)], \quad (5)$$

where m_0 is the chiral mass of the pion, Φ_π^{T2} and Φ_π^{T3} denote the pion meson wave function at the twist-2 and twist-3 levels, the dimensionless vectors are defined by $n_+ = (1, 0, \mathbf{0}_T)$ and $n_- = (0, 1, \mathbf{0}_T)$, and N_c is the number of colors. Without considering the transverse component of the B meson spin projector, the LO twist-3 contribution for Fig. 1(a) is of the form

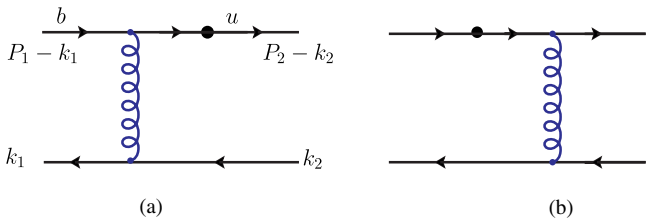

FIG. 1 (color online). Leading-order quark diagrams for the $B \to \pi$ transition form factor with the symbol circle in (a) and (b) representing the weak vertex of the $B \to \pi l \bar{\nu}_l$ decay.

$$H^{(0)}_{\mathrm{a,T3}}(x_1,k_{1\mathrm{T}},x_2,k_{2\mathrm{T}}) = \frac{g_s^2 C_F m_0 m_B}{[(p_1-k_2)^2-m_B^2][(k_1-k_2)^2]} \times \left\{\phi_\pi^P(x_2)\left[\phi_B^+(x_1)\left(4\frac{p_2^\mu}{\eta}-4x_2p_2^\mu\right)+\phi_B^-(x_1)\left(4p_1^\mu-4x_2p_2^\mu-4\frac{p_2^\mu}{\eta}\right)\right] + \phi_\pi^T(x_2)\left[\phi_B^+(x_1)\left(4\frac{p_2^\mu}{\eta}-4x_2p_2^\mu\right)+\phi_B^-(x_1)\left(4\frac{p_2^\mu}{\eta}-4p_1^\mu-4x_2p_2^\mu\right)\right]\right\}, \quad (6)$$

and for Fig. 1(b), we find

$$H^{(0)}_{\mathrm{b,T3}}(x_1,k_{1\mathrm{T}},x_2,k_{2\mathrm{T}}) = \frac{2g_s^2 C_F m_0 m_B \phi_\pi^P(x_2)}{[(p_2-k_1)^2][(k_1-k_2)^2]}[4p_2^\mu\phi_B^+(x_1)-4x_1p_1^\mu\phi_B^-(x_1)], \quad (7)$$

where $C_F = 4/3$ is the color factor.

The LO twist-2 contributions for Figs. 1(a) and 1(b) are of the form

$$H^{(0)}_{\mathrm{a,T2}}(x_1,k_{1\mathrm{T}},x_2,k_{2\mathrm{T}}) = -4g_s^2 C_F m_B^2 \phi_\pi^A(x_2)\frac{p_2^\mu\phi_B^-(x_1)+k_2^\mu\phi_B^+(x_1)}{[(p_1-k_2)^2-m_B^2][(k_1-k_2)^2]}, \quad (8)$$

$$H^{(0)}_{\mathrm{b,T2}}(x_1,k_{1\mathrm{T}},x_2,k_{2\mathrm{T}}) = -4g_s^2 C_F m_B^2 \phi_\pi^A(x_2)x_1\frac{(\eta p_1^\mu-p_2^\mu)\phi_B^+(x_1)+p_2^\mu\phi_B^-(x_1)}{[(p_2-k_1)^2][(k_1-k_2)^2]}. \quad (9)$$

For the LO twist-2 hard kernel $H^{(0)}_{\mathrm{b,T2}}$, it is strongly suppressed by the small x_2, as can be seen easily from Eqs. (8) and (9), and, therefore, the $H^{(0)}_{\mathrm{a,T2}}$ from Fig. 1(a) is the dominant part of the full LO twist-2 contribution. Consequently, it is reasonable to consider the NLO twist-2 contributions from Fig. 1(a) only in the calculation for the NLO twist-2 contributions.

For the LO twist-3 hard kernel $H^{(0)}_{\mathrm{b,T3}}$, the first term proportional to $p_2^\mu\phi_B^+(x_1)$ in Eq. (7) provides the dominant contribution, while the second term proportional to $x_1p_1^\mu\phi_B^-0(x_1)$ is strongly suppressed by the small x_1. The $H^{(0)}_{\mathrm{a,T3}}$ can be neglected safely when compared with $H^{(0)}_{\mathrm{b,T3}}$, due to the strong suppression of small x_1. Therefore, we consider only the $\phi_\pi^P(x_2)$ component in Eq. (7) from Fig. 1(b) in our estimation for the NLO twist-3 contribution.

The LO hard kernels given in Eqs. (6)–(9) are consistent with those given in Refs. [21,22], where the B meson wave function was defined as

$$-\frac{1}{\sqrt{2N_c}}(\not{p}_1+m_B)\gamma_5\left[\phi_B(x_1)-\frac{\not{n}_+-\not{n}_-}{\sqrt{2}}\bar{\phi}_B(x_1)\right], \quad (10)$$

with the relations

$$\phi_B = \frac{1}{2}(\phi_B^+ + \phi_B^-), \qquad \bar{\phi}_B = \frac{1}{2}(\phi_B^+ - \phi_B^-). \quad (11)$$

By comparing the hard kernel $H^{(0)}_{\mathrm{b,T3}}$ in Eq. (7) with $H^{(0)}_{\mathrm{a,T2}}$ in Eq. (8), one can find that the LO twist-3 contribution is enhanced by the factor $1/x_1$ and the pion chiral mass $m_0^\pi > 1$, and, consequently, larger than the LO twist-2 contribution which is associated with the factor $1/x_2$. The numerical results of Eqs. (7) and (8) in the large recoil region also show that the LO twist-3 contribution is larger than the LO twist-2 part, by a ratio of around 60% over 40%. This fact means that the NLO twist-3 contribution may be important when compared with the corresponding NLO twist-2 one; this is one of the motivations for us to make the evaluation for the NLO twist-3 contribution to the $B \to \pi$ form factor.

III. NLO CORRECTIONS

Since the dominant NLO twist-3 contribution to the form factor of the $B \to \pi$ transition is proportional to the $\phi_\pi^P(x_2)\phi_B^+(x_1)$ from Fig. 1(b), here we consider only the NLO corrections to Fig. 1(b) coming from the quark-level corrections and the wave function corrections at the twist-3 level to find the NLO twist-3 contribution to the form factor of the $B \to \pi$ transition.

Under the hierarchy in Eq. (2), only the terms that do not vanish in the limits of $x_i \to 0$ and $k_{iT}^2 \to 0$ are kept to simplify the expressions of the NLO twist-3 contributions greatly.

A. NLO corrections from the QCD quark diagrams

The NLO corrections to Fig. 1(b) at the quark level contain the self-energy diagrams, the vertex diagrams, and the box and pentagon diagrams, as illustrated by Figs. 2, 3, and 4, respectively. The ultraviolet (UV) divergences are extracted in the dimensional reduction [23] in order to avoid the ambiguity from handling the matrix γ_5. The infrared (IR) divergences are identified as the logarithms $\ln m_g$, $\ln\delta_1$, and $\ln\delta_2$ and their combinations, where the dimensionless ratios are adopted,

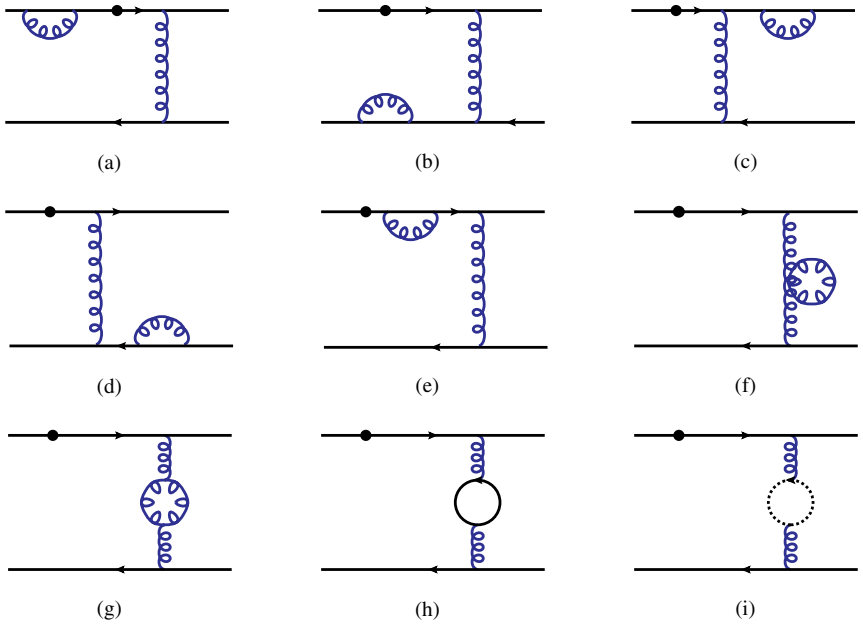

FIG. 2 (color online). The Feynman diagrams (a)–(i), they provide the self-energy corrections to Fig. 1(b).

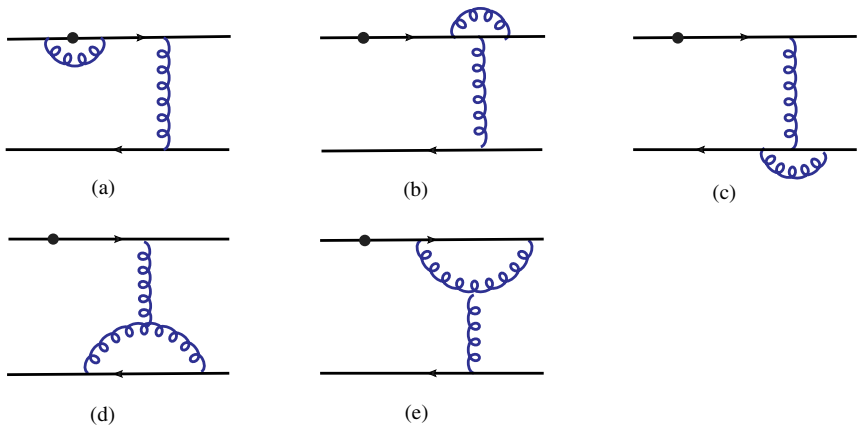

FIG. 3 (color online). The Feynman diagrams (a)–(e), they provide the vertex corrections to Fig. 1(b).

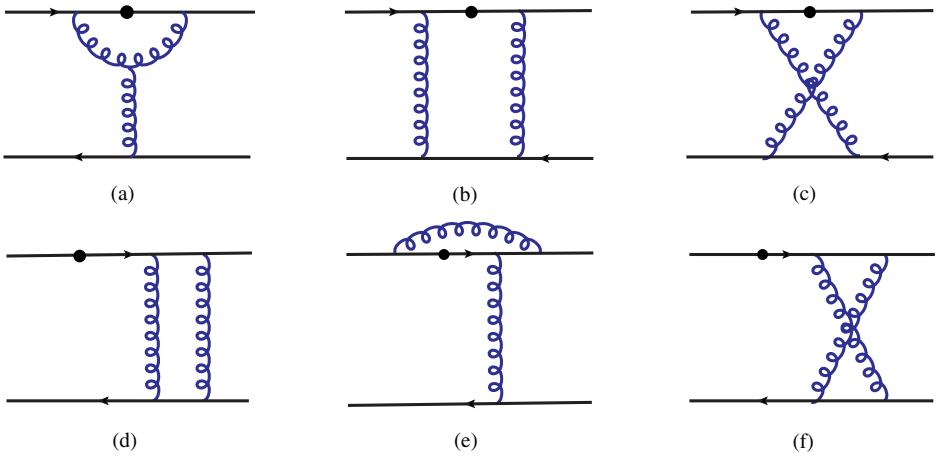

FIG. 4 (color online). The Feynman diagrams (a)–(f), they provide the box and pentagon corrections to Fig. 1(b).

$$\delta_1 = \frac{k_{1\mathrm{T}}^2}{m_B^2}, \qquad \delta_2 = \frac{k_{2\mathrm{T}}^2}{m_B^2}, \qquad \delta_{12} = \frac{-(k_1-k_2)^2}{m_B^2}. \tag{12}$$

By analytical evaluations for the Feynman diagrams, as shown in Fig. 2, we find the self-energy corrections from the nine diagrams:

$$G_{2a}^{(1)} = -\frac{\alpha_s C_f}{4\pi}\left[\frac{6}{\delta_1}\left(\frac{1}{\epsilon}+\ln\frac{4\pi\mu^2}{m_B^2 e^{\gamma_E}}+\frac{1}{3}\right) + \frac{1}{2}\left(\frac{1}{\epsilon}+\ln\frac{4\pi\mu^2}{m_B^2 e^{\gamma_E}}+2\ln\frac{m_g^2}{m_B^2}+2\right)\right]H^{(0)}, \tag{13}$$

$$G_{2b}^{(1)} = -\frac{\alpha_s C_f}{8\pi}\left[\frac{1}{\epsilon}+\ln\frac{4\pi\mu^2}{\delta_1 m_B^2 e^{\gamma_E}}+2\right]H^{(0)}, \tag{14}$$

$$G_{2c,2d}^{(1)} = -\frac{\alpha_s C_f}{8\pi}\left[\frac{1}{\epsilon}+\ln\frac{4\pi\mu^2}{\delta_2 m_B^2 e^{\gamma_E}}+2\right]H^{(0)}, \tag{15}$$

$$G_{2e}^{(1)} = -\frac{\alpha_s C_f}{4\pi}\left[\frac{1}{\epsilon}+\ln\frac{4\pi\mu^2}{x_1\eta m_B^2 e^{\gamma_E}}+2\right]H^{(0)}, \tag{16}$$

$$G_{2f+2g+2h+2i}^{(1)} = \frac{\alpha_s}{4\pi}\left[\left(\frac{5}{3}N_c-\frac{2}{3}N_f\right)\left(\frac{1}{\epsilon}+\ln\frac{4\pi\mu^2}{\delta_{12} m_B^2 e^{\gamma_E}}\right)\right]H^{(0)}, \tag{17}$$

where $1/\epsilon$ represents the UV pole, μ is the renormalization scale, γ_E is the Euler constant, N_c is the number of the quark color, N_f is the number of the quarks flavors, and $H^{(0)}$ denotes the first term of the LO twist-3 contribution $H_{\mathrm{b,T3}}^{(0)}(x_1, k_{1\mathrm{T}}, x_2, k_{2\mathrm{T}})$ as given in Eq. (7),

$$H^{(0)}(x_1, k_{1\mathrm{T}}, x_2, k_{2\mathrm{T}}) = -4g_s^2 C_F m_0 m_B \phi_\pi^P(x_2)\frac{2p_2^\mu \phi_B^+(x_1)}{(p_2-k_1)^2(k_1-k_2)^2}. \tag{18}$$

It is easy to see that, besides $G_{2e}^{(1)}$ for Fig. 2(e), the NLO self-energy corrections listed in Eqs. (14), (15), and (17) are identical to the self-energy corrections for the NLO twist-2 case as given in Eqs. (7), (8), and (11) in Ref. [15]. Except for a small difference in the constant numbers, the $G_{2a}^{(1)}$ for Fig. 2(a) in Eq. (13) is the same one as that given in Eq. (7) of Ref. [15] for the case of the NLO twist-2 contributions. The reason for such high similarity is that the self-energy diagrams do not involve the loop momentum flow into the hard kernel. Only Fig. 2(a), the self-energy correction of the b quark, is emphasized here. The first term in the square brackets of $G_{2a}^{(1)}$ required the mass renomalization, and the finite piece of the first term is then absorbed into the redefinition of the b quark mass, with the relation $(p_1-k_1)^2 - m_B^2 = -k_{1\mathrm{T}}^2$. The second term in the square brackets of $G_{2a}^{(1)}$ represents the correction to the b quark wave function. The involved soft divergence is regularized by the gluon mass m_g because the valence b quark is considered on shell, and the additional regulator m_g will be canceled by the corresponding soft divergence in the effective diagram [Fig. 5(a)]. Comparing with the NLO twist-2 case, the result from Fig. 2(e) at twist-3 is simple, since it is the self-energy correction to the massless internal quark line in the twist-3 case.

By analytical evaluations for the Feynman diagrams as shown in Fig. 3, we find the vertex corrections from the five vertex diagrams:

$$G_{3a}^{(1)} = \frac{\alpha_s C_f}{4\pi}\times\left[\frac{1}{\epsilon}+\ln\frac{4\pi\mu^2}{m_B^2 e^{\gamma_E}}-\ln^2 x_1 - 2\ln x_1(1-\ln\eta)-\frac{2\pi^2}{3}-1\right]H^{(0)}, \tag{19}$$

$$G_{3b}^{(1)} = -\frac{\alpha_s}{8\pi N_c}\left[\frac{1}{\epsilon}+\ln\frac{4\pi\mu^2}{x_1\eta m_B^2 e^{\gamma_E}}-\frac{1}{2}\right]H^{(0)}, \tag{20}$$

$$G_{3c}^{(1)} = -\frac{\alpha_s}{8\pi N_c}\times\left[\frac{1}{\epsilon}+\ln\frac{4\pi\mu^2}{\delta_{12} m_B^2 e^{\gamma_E}}-\ln\frac{\delta_2}{\delta_{12}}\ln\frac{\delta_1}{\delta_{12}}-\ln\frac{\delta_1\delta_2}{\delta_{12}^2}-\frac{\pi^2}{3}\right]H^{(0)}, \tag{21}$$

$$G_{3d}^{(1)} = \frac{\alpha_s N_c}{8\pi}\left[\frac{3}{\epsilon}+3\ln\frac{4\pi\mu^2}{\delta_{12} m_B^2 e^{\gamma_E}}-\ln\frac{\delta_1\delta_2}{\delta_{12}^2}+\frac{11}{2}-\frac{2\pi^2}{3}\right]H^{(0)}, \tag{22}$$

$$G_{3e}^{(1)} = \frac{\alpha_s N_c}{8\pi}\left[\frac{3}{\epsilon}+3\ln\frac{4\pi\mu^2}{x_1\eta m_B^2 e^{\gamma_E}} - \ln\frac{\delta_2}{x_1\eta}(\ln x_2+1)+\frac{1}{2}\ln x_2-\frac{\pi^2}{3}+\frac{7}{4}\right]H^{(0)}. \tag{23}$$

The amplitude $G_{3a}^{(1)}$ has no IR divergence due to the fact that the radiative gluon attaches to the massive b quark and the internal line in Fig. 3(a). The amplitude $G_{3b}^{(1)}$ should have collinear divergence at first sight because the radiative gluon in Fig. 3(b) attaches to the light valence quark, but since it was found that the collinear region $l \| p_2$ was suppressed, then $G_{3b}^{(1)}$ is IR finite. The radiative gluon in Fig. 3(c) attaches to the light valence antiquarks, so that both the collinear and soft divergences are produced in $G_{3c}^{(1)}$, where the large double logarithm $\ln\delta_1 \ln\delta_2$ denoted as the overlap of the IR divergences can be absorbed into the B meson or the pion meson wave functions. The radiative gluon in Fig. 3(d) attaches to the light valence antiquarks as well as the virtual LO hard gluon, so the soft divergence and the large double logarithm are not generated in $G_{3d}^{(1)}$. The radiative gluon in Fig. 3(e) attaches only to the light valence quark as well as the virtual LO hard gluon, and then $G_{3e}^{(1)}$ just contains the collinear divergence regulated by $\ln\delta_2$ from the $l \| p_2$ region.

The analytical results from the box and pentagon diagrams as shown in Fig. 4 are summarized as

$$G_{4a}^{(1)} = -\frac{\alpha_s N_c}{8\pi} x_1 \left[\ln\frac{x_2\eta^2}{\delta_2} + 1\right] H^{(0)}, \tag{24}$$

$$G_{4b}^{(1)} = -\frac{\alpha_s C_f}{4\pi} \left[\ln^2\frac{\delta_1}{x_1^2} - \ln^2 x_1 - \frac{7\pi^2}{3}\right] H^{(0)}, \tag{25}$$

$$G_{4c}^{(1)} = -\frac{\alpha_s}{8\pi N_c} \left[\ln\frac{\delta_1}{\delta_{12}}\ln\frac{\delta_2}{\delta_{12}} - \frac{\pi^2}{12}\right] H^{(0)}, \tag{26}$$

$$G_{4d}^{(1)} = -\frac{\alpha_s C_F}{2\pi} \left[\ln\frac{\delta_1}{\delta_{12}}\ln\frac{\delta_2}{\delta_{12}} + \frac{\pi^2}{3}\right] H^{(0)}, \tag{27}$$

$$G_{4e}^{(1)} = \frac{\alpha_s}{8\pi N_c} \left[\ln\frac{\delta_1}{\eta}\ln\frac{\delta_2}{\eta} + \ln\delta_2 + \frac{\pi^2}{6}\right] H^{(0)}, \tag{28}$$

$$G_{4f}^{(1)} = -\frac{\alpha_s}{8\pi N_c} \left[\ln\frac{\delta_1}{\eta}\ln\frac{\delta_2}{\eta} - \ln x_2 \ln\delta_2 - \ln x_2 \ln\delta_{12} + \frac{1}{2}\ln^2\eta + \frac{1}{2}\ln^2\delta_{12} - \frac{1}{2}\ln^2 x_2 - \frac{\pi^2}{3} - 1\right] H^{(0)}. \tag{29}$$

Note that the amplitude of Fig. 4(a) has no IR divergence because the additional gluon is linked to the massive b quark and the virtual LO hard kernel gluon. Figure 4(b) is a two-particle reducible diagram, whose IR contribution would be canceled by the corresponding effective diagram for the B meson function Fig. 5(c). All the other four subdiagrams [Figs. 5(c)–5(f)] would generate double logarithms from the overlap region of the soft and collinear region, because the radiative gluon attached with the b quark and light valence quark generate both collinear divergence and soft divergence, as well as the gluon attached to two light valence partons. Figure 4(d) is also a two-particle reducible diagram, whose contribution should be canceled completely by the corresponding effective diagram [Fig. 5(c)] for the pion meson function due to the requirement of the factorization theorem. It is found that the double logarithm in Fig. 4(c) offset with the double logarithm in Fig. 3(c) and the cancellation would also appear for the double logarithms in Figs. 4(e) and 4(f).

The NLO twist-3 corrections from all three kinds of QCD quark diagrams are summed into

$$\begin{aligned} G^{(1)} = \frac{\alpha_s C_f}{4\pi}\Bigg\{ & \frac{21}{4}\left(\frac{1}{\epsilon} + \ln\frac{4\pi\mu^2}{m_B^2 e^{\gamma_E}}\right) - \ln^2\delta_1 - 2\ln\delta_1\ln\delta_2 - \frac{97}{16}\ln^2 x_1 - \frac{15}{8}\ln^2 x_2 \\ & + \frac{1}{2}(-1 + 12\ln x_1 + 4\ln x_2 + 4\ln\eta)\ln\delta_1 + (-1 + 2\ln x_1 + \ln x_2 + 2\ln\eta)\ln\delta_2 \\ & - \frac{23}{8}\ln x_1\ln x_2 - \frac{1}{8}(41 + 17\ln\eta)\ln x_1 - \frac{1}{16}(41 + 46\ln\eta)\ln x_2 \\ & - \frac{1}{96}[-273 + \pi^2 + 96\ln r_g + 12\ln\eta(25 + 17\ln\eta)]\Bigg\} H^{(0)} \end{aligned} \tag{30}$$

for $N_f = 6$. The UV divergence in the above expression is the same as in the pion electromagnetic form factor [14] and in the leading twist of the $B \to \pi$ transition form factor [15], which determines the renormalization-group evolution of the coupling constant α_s. The double logarithm that arose from the reducible subdiagrams Figs. 4(b) and 4(d) would be absorbed into the NLO wave functions.

B. NLO corrections of the effective diagrams

As pointed out in Ref. [15], a basic argument of k_T factorization is that the IR divergences arisen from the NLO corrections can be absorbed into the nonperturbative wave functions which are universal. From this point, the convolution of the NLO wave function $\Phi_B^{(1)}$ and the LO hard kernel $H^{(0)}$, the LO hard kernel $H^{(0)}$ and the NLO wave function $\Phi_\pi^{(1)}$ are computed, and then they cancel the IR divergences in the NLO amplitude $G^{(1)}$ as given in Eq. (30). The convolutions for the NLO wave functions and the LO hard kernel are calculated in this subsection. In the k_T factorization theorem, the $\Phi_B^{(1)}$ [24] collects the $O(\alpha_s)$ effective diagrams from the matrix elements of the leading Fock states $\Phi_B(x_1, k_{1T}; x_1', k_{1T}')$ and $\Phi_{\pi,P}^{(1)}$ collects the $O(\alpha_s)$ effective diagrams for the twist-3 transverse-momenta-dependent light-cone wave function $\Phi_{\pi,P}(x_2, k_{2T}; x_2', k_{2T}')$ [25,26]

$$\begin{aligned} &\Phi_B(x_1, k_{1T}; x_1', k_{1T}') \\ &= \int \frac{dz^-}{2\pi}\frac{d^2 z_T}{(2\pi)^2} e^{-ix_1' P_1^+ z^- + i\mathbf{k}_{1T}'\cdot\mathbf{z}_T} \\ &\quad \times \langle 0|\bar{q}(z) W_z(n_1)^\dagger I_{n_1;z,0} W_0(n_1) \hat{n}_+ \Gamma h_v(0)|h_v \bar{d}(k_1)\rangle, \end{aligned} \tag{31}$$

$$\begin{aligned} &\Phi_{\pi,P}(x_2, k_{2T}; x_2', k_{2T}') \\ &= \int \frac{dy^+}{2\pi}\frac{d^2 y_T}{(2\pi)^2} e^{-ix_2' P_2^- y^+ + i\mathbf{k}_{2T}'\cdot\mathbf{y}_T} \\ &\quad \times \langle 0|\bar{q}(y) W_y(n_2)^\dagger I_{n_2;y,0} W_0(n_2)\gamma_5 q(0)|u(p_2 - k_2)\bar{d}(k_2)\rangle, \end{aligned} \tag{32}$$

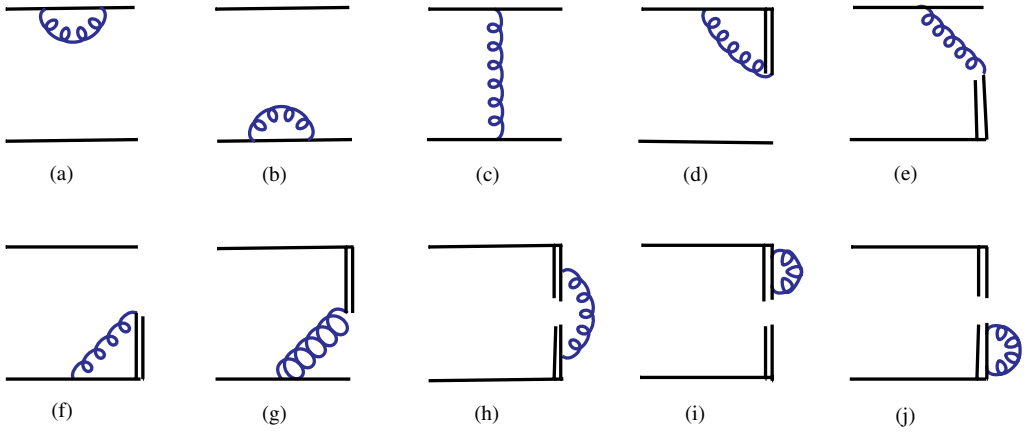

FIG. 5 (color online). The $O(\alpha_s)$ effective diagrams (a)–(j) for the B meson wave function.

respectively, in which $z = (0, z_-, \mathbf{z}_T)$ and $y = (y^+, 0, \mathbf{y}_T)$ are the light cone (LC) coordinates of the antiquark field $\bar{d}$ with the momentum fraction x_i, and h_ν is the effective heavy-quark field,

$$W_z(n_1) = \mathrm{P}\exp\left[-ig_s\int_0^\infty d\lambda n_1\cdot A(z+\lambda n_1)\right], \quad (33)$$

$$W_y(n_2) = \mathrm{P}\exp\left[-ig_s\int_0^\infty d\lambda n_2\cdot A(y+\lambda n_2)\right], \quad (34)$$

where P is the path ordering operator. The two Wilson lines $W_{y/z}(n_i)$ and $W_0(n_i)$ are connected by a vertical link $I_{n_i;y/z,0}$ at infinity [27]. Then the additional LC singularities from the region where the loop momentum $l\|n_-(n_+)$ [28] is regulated by the IR regulator n_1^2 and n_2^2. The scales $\xi_1^2 \equiv 4(n_1\cdot p_1)^2/|n_1^2| = m_B^2|n_1^-/n_1^+|$ and $\xi_2^2 \equiv 4(n_2\cdot p_2)^2/|n_2^2| = \eta^2 m_B^2|n_2^+/n_2^-|$ are introduced to avoid the LC singularity [15,29]. It is important to emphasize that the variation of the above scales is regarded as a factorization scheme dependence, which would be brought into the NLO hard kernel after taking the difference between the QCD quark diagrams and the effective diagrams. Additionally, the above scheme-dependent scales can be minimized by adhering to fixed n_1^2 and n_2^2. In Ref. [16], very recently, Li *et al.* studied the joint resummation for the pion wave function and pion transition form factor, i.e., summing up the mixed logarithm $\ln(x_i)\ln(k_T)$ to all orders. Such joint resummation can reduce the above scheme dependence effectively.

The convolution for the $O(\alpha_s)$ order of the B meson function in Eq. (31) and $H^{(0)}$ over the integration variables x_1' and $k_{1\mathrm{T}}'$ is

$$\Phi_B^{(1)}\otimes H^{(0)} \equiv \int dx_1' d^2\mathbf{k}_{1\mathrm{T}}'\Phi_B^{(1)} \times (x_1, \mathbf{k}_{1\mathrm{T}}; x_1', \mathbf{k}_{1\mathrm{T}}')H^{(0)}(x_1', \mathbf{k}_{1\mathrm{T}}'; x_2, \mathbf{k}_{2\mathrm{T}}). \quad (35)$$

In the evolution, the n_1 is approximated to vector n_- with a very small plus component n_1^+ to avoid the LC singularity in the integration, and we choose n_1^- to be positive while n_1^+ can be positive or negative for convenience. The NLO twist-3 corrections from the $O(\alpha_s)$ order wave function as shown in Fig. 5 are listed in the following, with μ_f being the factorization scale:

$$\Phi_{5a}^{(1)}\otimes H^{(0)} = \frac{\alpha_s C_f}{4\pi}\left[\frac{1}{\epsilon} + \ln\frac{4\pi\mu_f^2}{m_B^2 e^{\gamma_E}} - \ln r_g\right]H^{(0)}, \quad (36)$$

$$\Phi_{5b}^{(1)}\otimes H^{(0)} = -\frac{\alpha_s C_f}{8\pi}\left[\frac{1}{\epsilon} + \ln\frac{4\pi\mu_f^2}{m_B^2 e^{\gamma_E}} - \ln\delta_1 + 2\right]H^{(0)}, \quad (37)$$

$$\Phi_{5c}^{(1)}\otimes H^{(0)} = -\frac{\alpha_s C_f}{4\pi}\left[\ln^2\left(\frac{\delta_1}{x_1^2}\right)\right]H^{(0)}, \quad (38)$$

$$\Phi_{5d}^{(1)}\otimes H^{(0)} = -\frac{\alpha_s C_f}{8\pi}(-\ln r_1) \times\left[\frac{1}{\epsilon} + \ln\frac{4\pi\mu_f^2}{m_B^2 e^{\gamma_E}} - \ln r_g\right]H^{(0)}, \quad (39)$$

$$\Phi_{5e}^{(1)}\otimes H^{(0)} = \frac{\alpha_s C_f}{4\pi}(-\ln r_1)[-\ln r_1 - \ln r_g + \frac{1}{2}\ln r_1 + 2\ln x_1]H^{(0)}, \quad (40)$$

$$\Phi_{5f}^{(1)}\otimes H^{(0)} = \frac{\alpha_s C_f}{8\pi}\left[\frac{1}{\epsilon} + \ln\frac{4\pi\mu_f^2}{m_B^2 e^{\gamma_E}} + \ln r_1 - 2\ln x_1 - (\ln\delta_1 - 2\ln x_1 + \ln r_1)^2 - 2(\ln\delta_1 - 2\ln x_1 + \ln r_1) - \frac{\pi^2}{3} + 2\right]H^{(0)}, \quad (41)$$

$$\Phi_{5g}^{(1)} \otimes H^{(0)} = \frac{\alpha_s C_f}{8\pi}\left[(\ln\delta_1 - 2\ln x_1 + \ln r_1)^2 - \frac{\pi^2}{3}\right]H^{(0)},$$
$$\times (\Phi_{5h}^{(1)} + \Phi_{5i}^{(1)} + \Phi_{5j}^{(1)}) \otimes H^{(0)}$$
$$= \frac{\alpha_s C_f}{4\pi}\left[\frac{1}{\epsilon} + \ln\frac{4\pi\mu_f^2}{m_B^2 e^{\gamma_E}} - \ln\delta_{12}\right]H^{(0)}, \quad (42)$$

where the dimensionless parameter $r_1 = m_B^2/\xi_1^2$ is chosen small to obtain the simple results as above. Because the two propagators in the LO hard kernel $H^{(0)}$ are both relevant to x_1' while only one is relevant to x_2', there exist three five-point integrals as shown in Figs. 5(c), 5(e), and 5(g) that need to be calculated. The reducible subdiagram Fig. 5(c) reproduced the double logarithm as the quark subdiagram Fig. 4(b). The difference between the effective heavy-quark field employed in the B meson wave function and the b quark field in the quark diagrams leads to different results in Figs. 4(b) and 5(c). It is found that the regulator $\ln m_g$ adopted to regularize the soft divergence in the reducible Fig. 5(a) will be canceled by Fig. 2(a), while the regulators $\ln m_g$ in Figs. 5(d) and 5(e) cancel each other. The large double logarithms $(\ln\delta_1 - 2\ln x_1 + \ln r_1)^2$ in Figs. 5(f) and 5(g) also cancel each other, so the other IR divergences are regulated only by $\ln\delta_1$ as the prediction because it is just the NLO correction to the incoming B meson wave function.

After summing all the $O(\alpha_s)$ contributions in Fig. 5, we obtain

$$\Phi_B^{(1)} \otimes H^{(0)} = \frac{\alpha_s C_f}{4\pi}\left[\frac{1}{2}(4 + \ln r_1)\left(\frac{1}{\epsilon} + \ln\frac{4\pi\mu_f^2}{m_B^2 e^{\gamma_E}}\right) - \ln^2\delta_1\right.$$
$$+ \frac{1}{2}(-1 + 8\ln x_1)\ln\delta_1 - \ln r_g - 4\ln^2 x_1$$
$$+ (1 - \ln r_1)\ln x_1 - \frac{1}{2}\ln r_1 + \frac{1}{4}\ln^2 r_1$$
$$\left. - \ln\delta_{12} - \frac{\pi^2}{3}\right]H^{(0)}. \quad (43)$$

The convolution of $H^{(0)}$ and the $O(\alpha_s)$ outgoing pion meson wave function $\Phi_\pi^{(1)}$ over the integration variables x_2' and k_{2T}' is

$$H^{(0)} \otimes \Phi_{\pi,P}^{(1)} \equiv \int dx_2' d^2\mathbf{k}_{2T}' H^{(0)}(x_1, \mathbf{k}_{1T}; x_2', \mathbf{k}_{2T}')\Phi_{\pi,P}^{(1)}$$
$$\times (x_2', \mathbf{k}_{2T}'; x_2, \mathbf{k}_{2T}). \quad (44)$$

The n_2 is mainly in an n_+ component, and a very small minus component n_2^- is kept to avoid the LC singularity. Note that the sign of n_2^+ is positive as P_1^+, while the sign of n_2^- is arbitrary for convenience.

Figure 6 collects all the NLO corrections to the outgoing pion wave function and $r_2 = m_B^2/\xi_2^2$. The reducible subdiagrams Figs. 5(a)–5(c) and 6(a)–6(c) generate the same results as in the leading twist-2 case [15], while the results from the irreducible subdiagrams Figs. 5(d)–5(j) and 6(d)–6(j) in the twist-3 are half smaller than that in the leading twist-2, due to their different spin structures. The amplitude of the reducible Fig. 6(c) convoluted by the LO hard kernel $H^{(0)}$ reproduced the double logarithm $\ln\delta_1\ln\delta_2$. There are no five-point integrals in $H^{(0)} \otimes \Phi^{(1)}$ because only one denominator in $H^{(0)}$ is relevant to x_2'. Then the most complicated integrals involved here are the four-point integrations attached to Figs. 6(e) and 6(g). The double logarithm in $H^{(0)} \otimes \Phi_{8d}^{(1)}$, $H^{(0)} \otimes \Phi_{8e}^{(1)}$, $H^{(0)} \otimes \Phi_{8f}^{(1)}$, and $H^{(0)} \otimes \Phi_{8g}^{(1)}$ are also canceled. Only a double logarithm $\ln\delta_1\ln\delta_2$, which would be canceled by the quark diagram Fig. 4(d), is still left in the $H^{(0)} \otimes \Phi_{\pi,P}^{(1)}$.

The analytical results from Fig. 6 are listed in the following, with μ_f being the factorization scale:

$$H^{(0)} \otimes \Phi_{6a}^{(1)} = -\frac{\alpha_s C_f}{8\pi}\left[\frac{1}{\epsilon} + \ln\frac{4\pi\mu_f^2}{m_B^2 e^{\gamma_E}} - \ln\delta_2 + 2\right]H^{(0)}, \quad (45)$$

$$H^{(0)} \otimes \Phi_{6b}^{(1)} = -\frac{\alpha_s C_f}{8\pi}\left[\frac{1}{\epsilon} + \ln\frac{4\pi\mu_f^2}{m_B^2 e^{\gamma_E}} - \ln\delta_2 + 2\right]H^{(0)}, \quad (46)$$

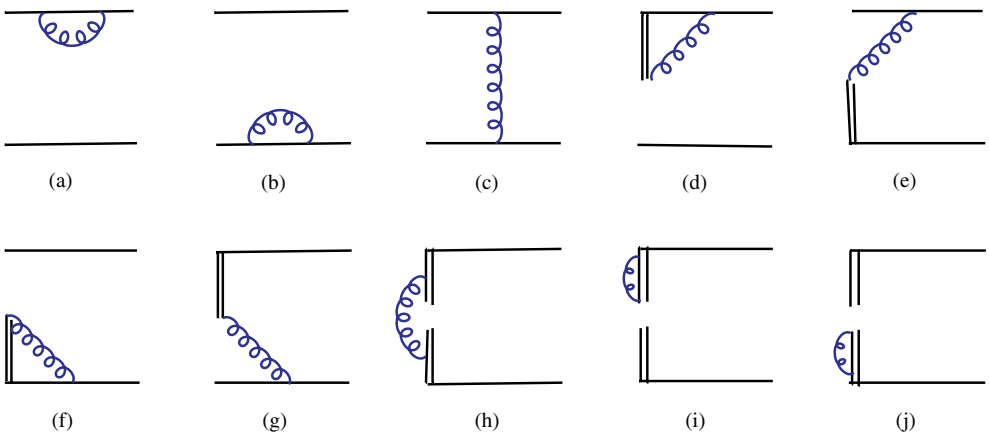

FIG. 6 (color online). The $O(\alpha_s)$ effective diagrams (a)–(j) for the π meson wave function.

$$H^{(0)} \otimes \Phi_{6c}^{(1)} = -\frac{\alpha_s C_f}{2\pi}\left[\ln\frac{\delta_{12}}{\delta_1}\ln\frac{\delta_{12}}{\delta_2}+\frac{\pi^2}{3}\right]H^{(0)}, \quad (47)$$

$$H^{(0)} \otimes \Phi_{6d}^{(1)} = \frac{\alpha_s C_f}{8\pi}\left[\frac{1}{\epsilon}+\ln\frac{4\pi\mu_f^2}{m_B^2 e^{\gamma_E}}-\ln\delta_2-(\ln r_2+\ln\delta_2)^2 - (\ln r_2+\ln\delta_2)+2-\frac{\pi^2}{3}\right]H^{(0)}, \quad (48)$$

$$H^{(0)} \otimes \Phi_{6e}^{(1)} = \frac{\alpha_s C_f}{8\pi}[(\ln x_2-\ln r_2-\ln\delta_2)^2+\pi^2]H^{(0)}, \quad (49)$$

$$H^{(0)} \otimes \Phi_{6f}^{(1)} = \frac{\alpha_s C_f}{8\pi}\left[\frac{1}{\epsilon}+\ln\frac{4\pi\mu_f^2}{m_B^2 e^{\gamma_E}}-\ln\delta_2 - (2\ln x_2-\ln r_2-\ln\delta_2)^2+(2\ln x_2-\ln r_2 - \ln\delta_2)+2-\frac{\pi^2}{3}\right]H^{(0)}, \quad (50)$$

$$H^{(0)} \otimes \Phi_{6g}^{(1)} = \frac{\alpha_s C_f}{8\pi}\left[(2\ln x_2-\ln r_2-\ln\delta_2)^2-\frac{\pi^2}{3}\right]H^{(0)}, \quad (51)$$

$$H^{(0)} \otimes (\Phi_{6h}^{(1)}+\Phi_{6i}^{(1)}+\Phi_{6j}^{(1)}) = \frac{\alpha_s C_f}{4\pi}\left[\frac{1}{\epsilon}+\ln\frac{4\pi\mu_f^2}{m_B^2 e^{\gamma_E}}-\ln\delta_{12}\right]H^{(0)}. \quad (52)$$

The total contributions from the convolution of the LO hard kernel and the NLO final pion meson wave function are obtained by summing all terms as given in the above equations:

$$H^{(0)} \otimes \Phi_{\pi,P}^{(1)} = \frac{\alpha_s C_f}{4\pi}\left[\left(\frac{1}{\epsilon}+\ln\frac{4\pi\mu_f^2}{m_B^2 e^{\gamma_E}}\right)-2\ln\delta_1\ln\delta_2 + 2\ln\delta_{12}\ln\delta_1-(1+\ln x_2-2\ln\delta_{12})\ln\delta_2 + \frac{1}{2}\ln^2(x_2)+(1-\ln r_2)\ln x_2 - \ln r_2-\ln\delta_{12}-2\ln^2\delta_{12}-\frac{2\pi^2}{3}\right]H^{(0)}. \quad (53)$$

C. NLO hard kernel

It is obvious that the UV poles are different in Eqs. (43) and (53), since the former involves the effective heavy-quark field instead of the b quark field. Then, the B meson and pion meson wave functions exhibit different evolution as proved in Ref. [15]. The $\ln\mu_f$ term in Eq. (43) was partly absorbed into the B meson wave function and partly to the B meson decay constant $f_B(\mu_f)$.

The IR-finite k_T-dependent NLO hard kernel for the $B \to \pi$ transition form factor at twist-3 is extracted by taking the difference between the contributions from the QCD quark diagrams and the contributions from the effective diagrams [30]:

$$H^{(1)}(x_1,\mathbf{k}_{1T};x_2,\mathbf{k}_{2T}) = G^{(1)}(x_1,\mathbf{k}_{1T};x_2,\mathbf{k}_{2T}) - \int dx_1' d^2\mathbf{k}_{1T}' \Phi_B^{(1)}(x_1,\mathbf{k}_{1T};x_1',\mathbf{k}_{1T}')H^{(0)}(x_1',\mathbf{k}_{1T}';x_2,\mathbf{k}_{2T}) - \int dx_2' d^2\mathbf{k}_{2T}' H^{(0)}(x_1,\mathbf{k}_{1T};x_2',\mathbf{k}_{2T}')\Phi_{\pi,P}^{(1)}(x_2',\mathbf{k}_{2T}';x_2,\mathbf{k}_{2T}). \quad (54)$$

The bare coupling constant α_s in Eqs. (30), (43), and (53) can be rewritten as

$$\alpha_s = \alpha_s(\mu_f) + \delta Z(\mu_f)\alpha_s(\mu_f), \quad (55)$$

in which the counterterm $\delta Z(\mu_f)$ is defined in the modified minimal subtraction ($\overline{\text{MS}}$) scheme. Inserting Eq. (55) into Eqs. (18), (30), (43), and (53) regularizes the UV poles in Eq. (54) through the multiplication $\delta Z(\mu_f)H^{(0)}$, and then the UV poles in Eqs. (43) and (53) are regulated by the counterterm of the quark field and by an additional counterterm in the $\overline{\text{MS}}$ scheme.

The NLO hard kernel $H^{(1)}$ for Fig. 1(b) at twist-3 is given by

$$H^{(1)} = \frac{\alpha_s(\mu_f)C_F}{4\pi}\left\{\frac{21}{4}\ln\frac{\mu^2}{m_B^2}-\frac{1}{2}(6+\ln r_1)\ln\frac{\mu_f^2}{m_B^2}-\frac{1}{16}\ln^2 x_1-\frac{3}{8}\ln^2 x_2 + \frac{9}{8}\ln x_1\ln x_2+\left(-\frac{33}{8}+\ln r_1+\frac{15}{8}\ln\eta\right)\ln x_1+\left(-\frac{25}{16}+\ln r_2+\frac{9}{8}\ln\eta\right)\ln x_2 + \frac{1}{2}\ln r_1-\frac{1}{4}\ln^2 r_1+\ln r_2-\frac{9}{8}\ln\eta-\frac{1}{8}\ln^2\eta+\frac{95\pi^2}{96}+\frac{273}{96}\right\}H^{(0)}. \quad (56)$$

The choice of the dimensionless scales ξ_1^2 and ξ_2^2 corresponds to a factorization scheme as discussed in the last subsection. The ξ_2^2 is fixed to m_B^2, and $\xi_1/m_B = 25$ is chosen in the numerical analysis to obtain the simplified results in Eqs. (39)–(42).

The additional double logarithm $\ln^2 x_1$ derived from the limit that the internal quark is on shell due to the tiny momentum fraction x_1 should be considered. It is absorbed into the jet function $J(x_1)$ [18,19]

$$J^{(1)}H^{(0)} = -\frac{1}{2}\frac{\alpha_s(\mu_f)C_F}{4\pi}\left[\ln^2(x_1) + \ln x_1 + \frac{\pi^2}{3}\right]H^{(0)}, \tag{57}$$

where the factor $1/2$ reflects the different spin structures of the twist-3 and twist-2 cases. The NLO hard kernel from Eq. (56) turns into the following format after subtracting the jet function in Eq. (57):

$$\begin{aligned} H^{(1)} &\to H^{(1)} - J^{(1)}H^{(0)} \\ &= \frac{\alpha_s(\mu_f)C_F}{4\pi}\left[\frac{21}{4}\ln\frac{\mu^2}{m_B^2} - \frac{1}{2}(6+\ln r_1)\ln\frac{\mu_f^2}{m_B^2} + \frac{7}{16}\ln^2 x_1 - \frac{3}{8}\ln^2 x_2\right. \\ &\quad + \frac{9}{8}\ln x_1 \ln x_2 + (-\frac{29}{8} + \ln r_1 + \frac{15}{8}\ln\eta)\ln x_1 + \left(-\frac{25}{16} + \ln r_2 + \frac{9}{8}\ln\eta\right)\ln x_2 \\ &\quad \left. + \frac{1}{2}\ln r_1 - \frac{1}{4}\ln^2 r_1 + \ln r_2 - \frac{9}{8}\ln\eta - \frac{1}{8}\ln^2\eta + \frac{37\pi^2}{32} + \frac{91}{32}\right]H^{(0)} \\ &= F_{\mathrm{T3}}^{(1)}(x_i, \mu, \mu_f, q^2)H^{(0)}, \end{aligned} \tag{58}$$

where $r_i = m_B^2/\xi_i^2$, $\eta = 1 - q^2/m_B^2$. The IR-finite k_T-dependent function $F_{\mathrm{T3}}^{(1)}(x_i, \mu, \mu_f, q^2)$ in Eq. (58) describes the NLO twist-3 contribution to the $B \to \pi$ transition form factors $f^+(q^2)$ and $f^0(q^2)$ as defined in Eq. (1).

IV. NUMERICAL ANALYSIS

In this section, the $B \to \pi$ transition form factors will be evaluated numerically up to twist-3 by employing the k_T factorization theorem, and the comparative analysis is developed between the LO and NLO as well as between the twist-2 and twist-3 NLO corrections.

In the calculation, the following nonasymptotic pion distribution amplitudes (DAs) as given in Refs. [31,32] will be used:

$$\begin{aligned} \phi_\pi^A(x) &= \frac{3f_\pi}{\sqrt{6}}x(1-x)[1 + a_2^\pi C_2^{\frac{3}{2}}(u) + a_4^\pi C_4^{\frac{3}{2}}(u)], \\ \phi_\pi^P(x) &= \frac{f_\pi}{2\sqrt{6}}\left[1 + \left(30\eta_3 - \frac{5}{2}\rho_\pi^2\right)C_2^{\frac{1}{2}}(u)\right. \\ &\quad \left. - 3\left(\eta_3\omega_3 + \frac{9}{20}\rho_\pi^2(1+6a_2^\pi)\right)C_4^{\frac{1}{2}}(u)\right], \\ \phi_\pi^T(x) &= \frac{f_\pi}{2\sqrt{6}}(1-2x)\left[1 + 6\left(5\eta_3 - \frac{1}{2}\eta_3\omega_3\right.\right. \\ &\quad \left.\left. - \frac{7}{20}\rho_\pi^2 - \frac{3}{5}\rho_\pi^2 a_2^\pi\right)(1 - 10x + 10x^2)\right], \end{aligned} \tag{59}$$

where $u = 2x - 1$, $m_\pi = 0.135$ GeV, $f_\pi = 0.13$ GeV, $m_0^\pi = 1.4$ GeV, and the Gegenbauer moments and Gegenbauer polynomials are adopted from Refs. [33,34],

$$\begin{aligned} &a_2^\pi = 0.25, \quad a_4^\pi = -0.015, \quad \rho_\pi = \frac{m_\pi}{m_0^\pi}, \\ &\eta_3 = 0.015, \quad \omega_3 = -3.0, \end{aligned} \tag{60}$$

$$\begin{aligned} C_2^{1/2} &= \frac{1}{2}(3u^2 - 1), \qquad C_2^{3/2} = \frac{3}{2}(5u^2 - 1), \\ C_4^{1/2} &= \frac{1}{8}(3 - 30u^2 + 35u^4), \\ C_4^{3/2} &= \frac{15}{8}(1 - 14u^2 + 21u^4). \end{aligned} \tag{61}$$

The B meson distribution amplitude widely used in the pQCD approach is of the form [21,22]

$$\phi_B(x,b) = \frac{f_B}{2\sqrt{6}}N_B x^2(1-x)^2 \cdot \exp\left[-\frac{x^2 m_B^2}{2\omega_B^2} - \frac{1}{2}(\omega_B b)^2\right], \tag{62}$$

where we have assumed that $\phi_B(x,b) = \phi_B^+(x,b) = \phi_B^-(x,b)$. The normalization condition of $\phi_B(x,b)$ is

$$\int_0^1 dx \phi_B(x, b=0) = \frac{f_B}{2\sqrt{2N_c}}, \tag{63}$$

with the mass $m_B = 5.28$ GeV, while the normalization constant $N_B = 100.921$ for $f_B = 0.21$ GeV and the fixed shape parameter $\omega_B = 0.40$.

The form factors $f^+(q^2)$ and $f^0(q^2)$ at the full LO level can be written as [21]

$$f^+(q^2)|_{\rm LO} = 8\pi m_B^2 C_F \int dx_1 dx_2 \int b_1 db_1 b_2 db_2 \phi_B(x_1,b_1) \times \Big\{ r_\pi[\phi_\pi^P(x_2) - \phi_\pi^T(x_2)] \cdot \alpha_s(t_1) \cdot e^{-S_{B\pi}(t_1)} \cdot S_t(x_2) \cdot h(x_1,x_2,b_1,b_2) + \left[(1+x_2\eta)\phi_\pi^A(x_2) + 2r_\pi\left(\frac{1}{\eta} - x_2\right)\phi_\pi^T(x_2) - 2x_2 r_\pi \phi_\pi^P(x_2)\right] \cdot \alpha_s(t_1) \cdot e^{-S_{B\pi}(t_1)} \cdot S_t(x_2) \cdot h(x_1,x_2,b_1,b_2) + 2r_\pi \phi_\pi^P(x_2) \cdot \alpha_s(t_2) \cdot e^{-S_{B\pi}(t_2)} \cdot S_t(x_1) \cdot h(x_2,x_1,b_2,b_1) \Big\}, \tag{64}$$

$$f^0(q^2)|_{\rm LO} = 8\pi m_B^2 C_F \int dx_1 dx_2 \int b_1 db_1 b_2 db_2 \phi_B(x_1,b_1) \times \Big\{ r_\pi(2-\eta)[\phi_\pi^P(x_2) - \phi_\pi^T(x_2)] \cdot \alpha_s(t_1) \cdot e^{-S_{B\pi}(t_1)} \cdot S_t(x_2) \cdot h(x_1,x_2,b_1,b_2) + [(1+x_2\eta)\eta\phi_\pi^A(x_2) + 2r_\pi(1-x_2\eta)\phi_\pi^T(x_2) - 2x_2\eta r_\pi \phi_\pi^P(x_2)] \cdot \alpha_s(t_1) \cdot e^{-S_{B\pi}(t_1)} \cdot S_t(x_2) \cdot h(x_1,x_2,b_1,b_2) + 2\eta r_\pi \phi_\pi^P(x_2) \cdot \alpha_s(t_2) \cdot e^{-S_{B\pi}(t_2)} \cdot S_t(x_1) \cdot h(x_2,x_1,b_2,b_1) \Big\}, \tag{65}$$

where $r_\pi = m_0^\pi/m_B$, the term proportional to ϕ_π^A denotes the LO twist-2 contribution, while those proportional to ϕ_π^P and ϕ_π^T make up the LO twist-3 contribution. The factor $\exp[-S_{B\pi}(t)]$ in Eqs. (64) and (65) contains the Sudakov logarithmic corrections and the renormalization group evolution effects of both the wave functions and the hard scattering amplitude with $S_{B\pi}(t) = S_B(t) + S_\pi(t)$, where

$$S_B(t) = s\left(x_1\frac{m_B}{\sqrt{2}}, b_1\right) + \frac{5}{3}\int_{1/b_1}^{t}\frac{d\bar{\mu}}{\bar{\mu}}\gamma_q(\alpha_s(\bar{\mu})),$$
$$S_\pi(t) = s\left(x_2\frac{m_B}{\sqrt{2}}, b_2\right) + s\left((1-x_2)\frac{m_B}{\sqrt{2}}, b_2\right) + 2\int_{1/b_2}^{t}\frac{d\bar{\mu}}{\bar{\mu}}\gamma_q(\alpha_s(\bar{\mu})), \tag{66}$$

with the quark anomalous dimension $\gamma_q = -\alpha_s/\pi$. The functions $s(Q,b)$ are defined by [21]

$$s(Q,b) = \frac{A^{(1)}}{2\beta_1}\hat{q}\ln\left(\frac{\hat{q}}{\hat{b}}\right) - \frac{A^{(1)}}{2\beta_1}(\hat{q}-\hat{b}) + \frac{A^{(2)}}{4\beta_1^2}\left(\frac{\hat{q}}{\hat{b}} - 1\right) - \left[\frac{A^{(2)}}{4\beta_1^2} - \frac{A^{(1)}}{4\beta_1}\ln\left(\frac{e^{2\gamma_E}-1}{2}\right)\right]\ln\left(\frac{\hat{q}}{\hat{b}}\right) + \frac{A^{(1)}\beta_2}{4\beta_1^3}\hat{q}\left[\frac{\ln(2\hat{q})+1}{\hat{q}} - \frac{\ln(2\hat{b})+1}{\hat{b}}\right] + \frac{A^{(1)}\beta_2}{8\beta_1^3}[\ln^2(2\hat{q}) - \ln^2(2\hat{b})], \tag{67}$$

where the variables are defined by $\hat{q} = \ln[Q/(\sqrt{2}\Lambda)]$, $\hat{b} = \ln[1/(b\Lambda)]$, and the coefficients $A^{(i)}$ and β_i are

$$\beta_1 = \frac{33-2n_f}{12}, \qquad \beta_2 = \frac{153-19n_f}{24}, \qquad A^{(1)} = \frac{4}{3},$$
$$A^{(2)} = \frac{67}{9} - \frac{\pi^2}{3} - \frac{10n_f}{27} + \frac{8}{3}\beta_1\ln(e^{\gamma_E}/2). \tag{68}$$

Here, n_f is the number of the quark flavors, and γ_E is the Euler constant. The hard scales t_i in the equations of this work are chosen as the largest scale of the virtuality of the internal particles in the hard b-quark decay diagram,

$$t_1 = \max\{\sqrt{x_2\eta}m_B, 1/b_1, 1/b_2\},$$
$$t_2 = \max\{\sqrt{x_1\eta}m_B, 1/b_1, 1/b_2\}. \tag{69}$$

The function $S_t(x)$ in Eqs. (64) and (65) is the threshold resummation factor that is adopted from Ref. [21]:

$$S_t(x) = \frac{2^{1+2c}\Gamma(3/2+c)}{\sqrt{\pi}\Gamma(1+c)}[x(1-x)]^c, \tag{70}$$

where we set the parameter $c = 0.3$. The hard functions $h(x_1,x_2,b_1,b_2)$ come from the Fourier transform of the hard kernel and can be written as [14]

$$h(x_1,x_2,b_1,b_2) = K_0(\sqrt{x_1x_2\eta}m_Bb_1)[\theta(b_1-b_2)I_0(\sqrt{x_2\eta}m_Bb_2)K_0(\sqrt{x_2\eta}m_Bb_1) + \theta(b_2-b_1)I_0(\sqrt{x_2\eta}m_Bb_1)K_0(\sqrt{x_2\eta}m_Bb_2)], \tag{71}$$

where I_0 and K_0 are the modified Bessel functions.

Before taking the NLO twist-3 contributions into account, we have to make a choice for the scales μ and μ_f, and try to minimize the NLO correction to the form

factor. Following Ref. [15], we also set $\mu_f = t$ with $t = t_1$ or t_2, the hard scale specified in the pQCD approach as given in Eq. (69), which is the largest energy scale in Figs. 1(a) or 1(b), respectively. The renormalization scale μ is chosen to diminish all the single logarithm and constant terms in the NLO hard kernel (58) [15]:

$$t_s(\mu_f) = \left\{ \mathrm{Exp}\left[c1 + \left(-\frac{9}{4} + \frac{1}{2}\ln r_1 \right) \ln \frac{\mu_f^2}{m_B^2} x_1^{c2} x_2^{c3} \right] \right\}^{2/21} \cdot \mu_f, \tag{72}$$

with the coefficients

$$\begin{aligned} c1 &= -\left(\frac{1}{2} - \frac{1}{4}\ln r_1 \right) \ln r_1 + \left(\frac{9}{8} + \frac{1}{8}\ln\eta \right) \ln\eta - \frac{379}{32} - \frac{167\pi^2}{96}, \\ c2 &= \frac{29}{8} - \ln r_1 - \frac{15}{8}\ln\eta, \\ c3 &= \frac{25}{16} - \frac{9}{8}\ln\eta \end{aligned} \tag{73}$$

based on our calculation.

When the NLO twist-2 and NLO twist-3 contributions to the $B \to \pi$ transition form factors are taken into account, the pQCD predictions for the two form factors at the full NLO level are of the form

$$\begin{aligned} f^+(q^2)|_{\mathrm{NLO}} = {} & 8\pi m_B^2 C_F \int dx_1 dx_2 \int b_1 db_1 b_2 db_2 \phi_B(x_1, b_1) \\ & \times \left\{ r_\pi [\phi_\pi^P(x_2) - \phi_\pi^T(x_2)] \cdot \alpha_s(t_1) \cdot e^{-S_{B\pi}(t_1)} \cdot S_t(x_2) \cdot h(x_1, x_2, b_1, b_2) \right. \\ & + \left[(1 + x_2\eta)(1 + F_{\mathrm{T2}}^{(1)}(x_i, t, q^2))\phi_\pi^A(x_2) + 2r_\pi \left(\frac{1}{\eta} - x_2 \right) \phi_\pi^T(x_2) - 2x_2 r_\pi \phi_\pi^P(x_2) \right] \\ & \times \cdot \alpha_s(t_1) \cdot e^{-S_{B\pi}(t_1)} \cdot S_t(x_2) \cdot h(x_1, x_2, b_1, b_2) \\ & \left. + 2r_\pi \phi_\pi^P(x_2)(1 + F_{\mathrm{T3}}^{(1)}(x_i, t, q^2)) \cdot \alpha_s(t_2) \cdot e^{-S_{B\pi}(t_2)} \cdot S_t(x_1) \cdot h(x_2, x_1, b_2, b_1) \right\}, \end{aligned} \tag{74}$$

$$\begin{aligned} f^0(q^2)|_{\mathrm{NLO}} = {} & 8\pi m_B^2 C_F \int dx_1 dx_2 \int b_1 db_1 b_2 db_2 \phi_B(x_1, b_1) \\ & \times \left\{ r_\pi (2 - \eta) [\phi_\pi^P(x_2) - \phi_\pi^T(x_2)] \cdot \alpha_s(t_1) \cdot e^{-S_{B\pi}(t_1)} \cdot S_t(x_2) \cdot h(x_1, x_2, b_1, b_2) \right. \\ & + [(1 + x_2\eta)(1 + F_{\mathrm{T2}}^{(1)}(x_i, t, q^2))\eta\phi_\pi^A(x_2) + 2r_\pi(1 - x_2\eta)\phi_\pi^T(x_2) - 2x_2\eta r_\pi \phi_\pi^P(x_2)] \\ & \times \cdot \alpha_s(t_1) \cdot e^{-S_{B\pi}(t_1)} \cdot S_t(x_2) \cdot h(x_1, x_2, b_1, b_2) \\ & \left. + 2\eta r_\pi (1 + F_{\mathrm{T3}}^{(1)}(x_i, t, q^2)) \phi_\pi^P(x_2) \cdot \alpha_s(t_2) \cdot e^{-S_{B\pi}(t_2)} \cdot S_t(x_1) \cdot h(x_2, x_1, b_2, b_1) \right\}, \end{aligned} \tag{75}$$

where the factor $F_{\mathrm{T2}}^{(1)}(x_i, t, q^2)$ describes the NLO twist-2 contribution as given in Ref. [15]

$$\begin{aligned} F_{\mathrm{T2}}^{(1)}(x_i, t, q^2) = {} & \frac{\alpha_s(\mu_f) C_F}{4\pi} \left[\frac{21}{4} \ln \frac{\mu^2}{m_B^2} - \left(\frac{13}{2} + \ln r_1 \right) \ln \frac{\mu_f^2}{m_B^2} + \frac{7}{16}\ln^2(x_1 x_2) + \frac{1}{8}\ln^2 x_1 \right. \\ & + \frac{1}{4}\ln x_1 \ln x_2 + \left(-\frac{1}{4} + 2\ln r_1 + \frac{7}{8}\ln\eta \right) \ln x_1 + \left(-\frac{3}{2} + \frac{7}{8}\ln\eta \right) \ln x_2 \\ & \left. + \frac{15}{4}\ln\eta - \frac{7}{16}\ln^2\eta + \frac{3}{2}\ln^2 r_1 - \ln r_1 + \frac{101\pi^2}{48} + \frac{219}{16} \right]. \end{aligned} \tag{76}$$

The factor $F_{\mathrm{T3}}^{(1)}(x_i, t, q^2)$ in Eqs. (74) and (75) denotes the NLO twist-3 contribution as defined in Eq. (58):

$$\begin{aligned} F_{\mathrm{T3}}^{(1)}(x_i, t, q^2) = {} & \frac{\alpha_s(\mu_f) C_F}{4\pi} \left[\frac{21}{4} \ln \frac{\mu^2}{m_B^2} - \frac{1}{2}(6 + \ln r_1) \ln \frac{\mu_f^2}{m_B^2} + \frac{7}{16}\ln^2 x_1 - \frac{3}{8}\ln^2 x_2 \right. \\ & + \frac{9}{8}\ln x_1 \ln x_2 + \left(-\frac{29}{8} + \ln r_1 + \frac{15}{8}\ln\eta \right) \ln x_1 + \left(-\frac{25}{16} + \ln r_2 + \frac{9}{8}\ln\eta \right) \ln x_2 \\ & \left. + \frac{1}{2}\ln r_1 - \frac{1}{4}\ln^2 r_1 + \ln r_2 - \frac{9}{8}\ln\eta - \frac{1}{8}\ln^2\eta + \frac{37\pi^2}{32} + \frac{91}{32} \right]. \end{aligned} \tag{77}$$

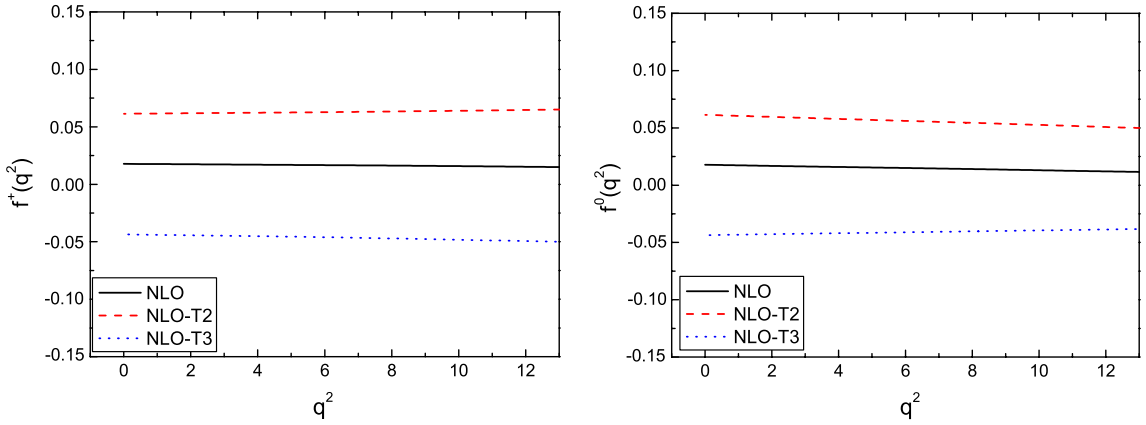

FIG. 7 (color online). The NLO twist-2 contribution (dashed curve), the NLO twist-3 contribution (dotted curve), and the total NLO contribution (solid curve) for $0 \le q^2 \le 12$ GeV^2 and setting $\mu_f = t$ and $\mu = t_s(\mu_f)$ as given in Eqs. (69) and (72).

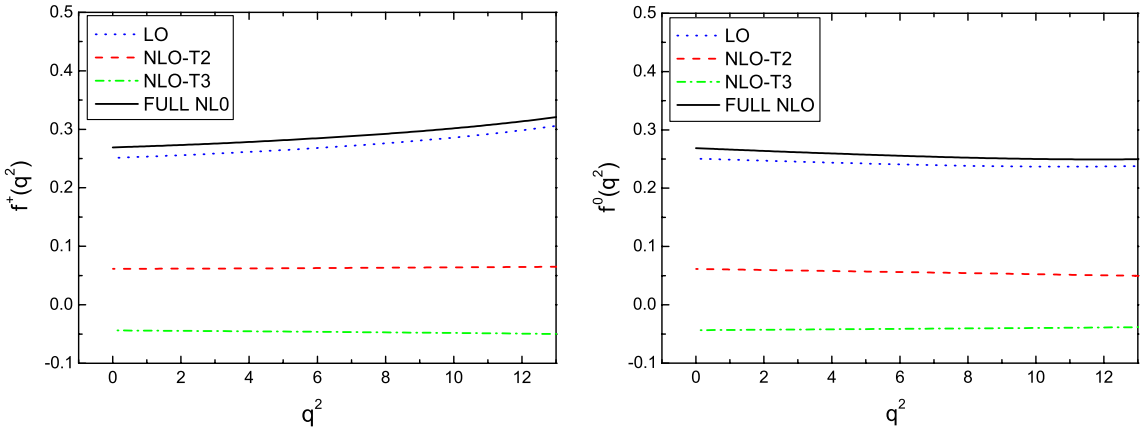

FIG. 8 (color online). The pQCD predictions for the form factors $f^+(q^2)$ and $f^0(q^2)$ assuming $\omega_B = 0.4$ and $c = 0.3$ and setting $\mu_f = t$ and $\mu = t_s(\mu_f)$. The left (right) diagram shows the q^2 dependence of the form factor, with the inclusion of the full LO contribution (dotted curve), the NLO twist-2 contribution only (dashed curve), the NLO twist-3 one only (dot-dashed curve), and, finally, the total contribution at the NLO level (solid curve).

The q^2 dependence of the form factors $f^+(q^2)$ and $f^0(q^2)$ in the k_T factorization up to NLO are shown in Figs. 7 and 8. In order to show and compare directly the relative strength of the contributions from different sources, we also list the pQCD predictions for the values of $f^+(q^2)$ and $f^0(q^2)$ in Table I, assuming $\omega_B = 0.40$, $c = 0.3$, and $q^2 = (0, 1, 3, 5, 7, 10, 12)$ GeV^2, respectively. In Table I, the labels "LO," "NLO-T2," "NLO-T3," and "NLO" mean

TABLE I. The pQCD predictions for the values of $f^+(q^2)$ and $f^0(q^2)$ for $\omega_B = 0.40$ and $c = 0.3$, and assuming $q^2 = (0, 1, 3, 5, 7, 10, 12)$ GeV^2. The labels LO, NLO-T2, NLO-T3, and NLO mean the full LO contribution, the NLO twist-2 part only, the NLO twist-3 part only, and the total contribution at the NLO level: the full LO plus both NLO twist-2 and twist-3 ones, respectively.

$f^+(q^2)$	0	1	3	5	7	10	12
LO	0.251	0.254	0.257	0.266	0.275	0.285	0.301
NLO-T2	0.061	0.061	0.062	0.063	0.063	0.064	0.064
NLO-T3	−0.043	−0.044	−0.044	−0.045	−0.046	−0.047	−0.048
NLO	0.269	0.271	0.275	0.284	0.294	0.302	0.317
$f^0(q^2)$	0	1	3	5	7	10	12
LO	0.251	0.248	0.246	0.243	0.239	0.237	0.236
NLO-T2	0.061	0.060	0.059	0.057	0.055	0.052	0.051
NLO-T3	−0.043	−0.043	−0.042	−0.042	−0.041	−0.040	−0.039
NLO	0.269	0.265	0.263	0.258	0.253	0.249	0.248

TABLE II. The pQCD predictions for various contributions $f_i^+(q^2)$ for $q^2 = (0, 5, 10)$ and their ratios $R_i(q^2) = f_i^+(q^2)/f_{\rm LO}^+(q^2)$.

Source	$f_i(0)$	$R_i(0)$	$f_i(5)$	$R_i(5)$	$f_i(10)$	$R_i(10)$
LO	0.251	100%	0.266	100%	0.285	100%
LO-T2	0.086	34.3%	0.084	31.6%	0.082	28.8%
NLO-T2	0.061	24.3%	0.063	23.7%	0.064	22.5%
LO-T3	0.165	65.7%	0.182	68.4%	0.203	71.2%
NLO-T3	−0.044	−17.1%	−0.045	−16.9%	−0.047	−16.5%
NLO	0.269	107.2%	0.284	106.8%	0.302	106.0%

the full LO contribution (LO twist-2 plus LO twist-3), the NLO twist-2 part only, the NLO twist-3 part only, and the total contribution at the NLO level (the full LO contribution plus both the NLO twist-2 and NLO twist-3 ones), respectively. In Table II, for the cases of $f^+(q^2)$ with $q^2 = (0, 5, 10)$ GeV^2, we show the pQCD predictions for various contributions to $f^+(q^2)$ from different sources: the LO twist-2, LO twist-3, NLO twist-2, NLO twist-3, and, finally, the total contribution at the NLO level. We also define the ratios $R_i = f_i^+(q^2)/f_{\rm LO}^+(q^2)$ to measure the relative percentage of different contributions with respect to the full LO contribution.

From the curves in Figs. 7 and 8 and the numerical results in Tables I and II, one can make the following observations:

(i) The NLO corrections at twist-2 and twist-3 are both under control, about 20% of the full LO contributions. The reason is that the end-point region of x_1 is

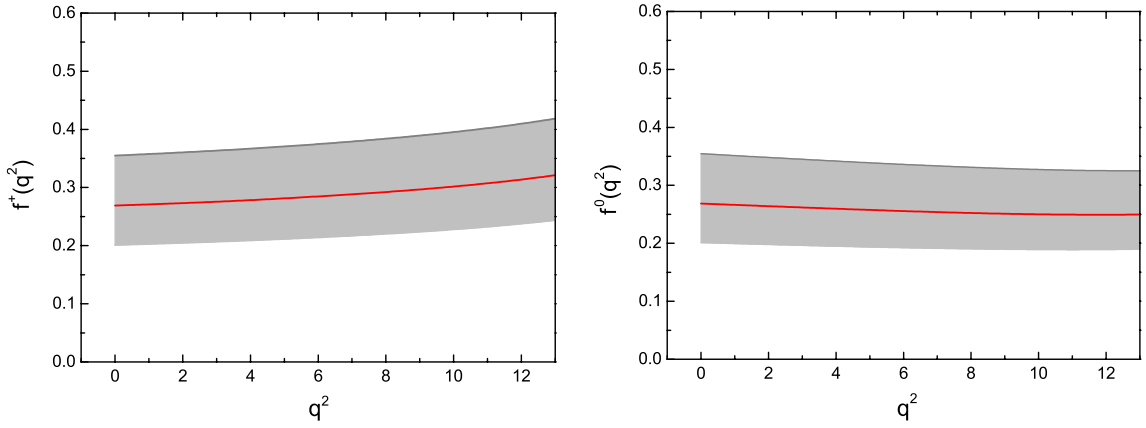

FIG. 9 (color online). Theoretical uncertainties of the $B \to \pi$ transition form factor with the choice $\mu_f = t$ and $\mu = t_s(\mu_f)$ in the range of $0 \le q^2 \le 12$ GeV^2.

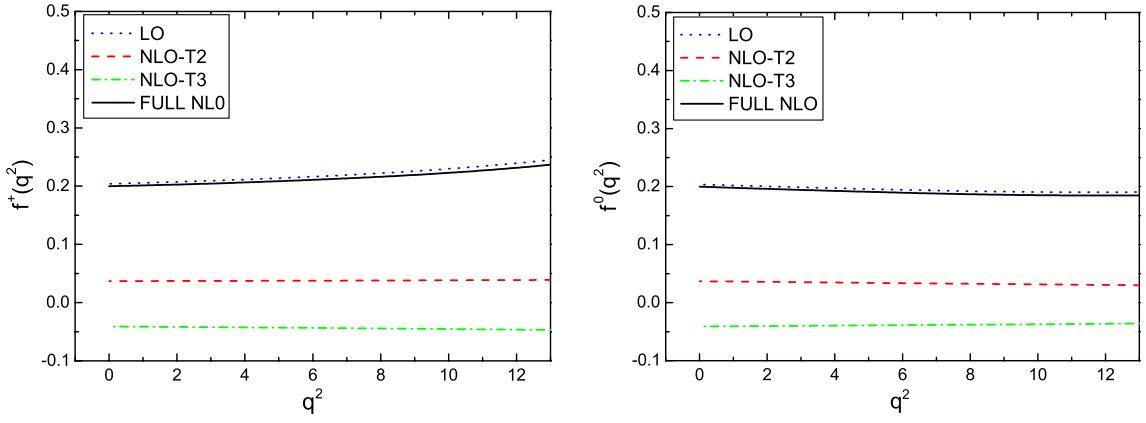

FIG. 10 (color online). The pQCD predictions for the form factors $f^+(q^2)$ and $f^0(q^2)$ for case B: the B meson DA in Eq. (62) and the asymptotic pion DAs in Eq. (80) are used in the numerical calculation.

TABLE III. The pQCD predictions for various contributions to $f_i^+(q^2)$ for $q^2 = (0, 5, 10)$ and their ratios $R_i(q^2) = f_i^+(q^2)/f_{\rm LO}^+(q^2)$ for case B.

Source	$f_i(0)$	$R_i(0)$	$f_i(5)$	$R_i(5)$	$f_i(10)$	$R_i(10)$
LO	0.204	100%	0.215	100%	0.230	100%
LO-T2	0.065	31.9%	0.063	29.3%	0.061	26.5%
NLO-T2	0.037	18.1%	0.038	17.7%	0.038	16.5%
LO-T3	0.139	68.1%	0.152	70.7%	0.168	73.0%
NLO-T3	−0.041	−20.1%	−0.043	−20.0%	−0.045	−19.6%
NLO	0.20	98.0%	0.210	97.7%	0.221	96.1%

strongly suppressed, and the large double logarithm $\ln^2 x_1$ in $H^{(1)}$ does not bring the dominant contribution in the NLO corrections at both twists.

(ii) From Fig. 7 and Tables I and II, one can see that the NLO twist-2 and NLO twist-3 contributions are similar in size but have an opposite sign, which leads to a strong cancellation between the NLO twist-2 and NLO twist-3 contributions and, consequently, results in a small total NLO contribution, as illustrated explicitly in Fig. 8. For the case of $f^+(0)$, for example, the LO twist-2 contribution is roughly half of the LO twist-3 part: 34% and 66% of the full LO contribution, respectively, while the NLO twist-2 contribution can provide an ∼24% enhancement to the LO prediction, but the NLO twist-3 part can provide an ∼17.5% decrease for the LO one. The total NLO contribution results in, consequently, a 7% enhancement to the LO $f^+(0)$ only.

(iii) Since the pQCD calculation for the form factors is reliable only at the low q^2 region, we, therefore, show the pQCD predictions for $f^+(q^2)$ and $f^0(q^2)$ in the region of $0 \le q^2 \le 12$ GeV^2 only. One can see from Figs. 7 and 8 that the pQCD predictions for the two form factors have a weak q^2 dependence: a 24% (22%) increase for the LO (NLO) prediction for $f^+(q^2)$, but an 8% (6%) decrease for the LO (NLO) prediction for $f^0(q^2)$, for the variation of q^2 from $q^2 = 0$ to $q^2 = 12$ GeV^2.

In our numerical calculations, the main theoretical errors come from the uncertainties of the input parameters $\omega_B = 0.40 \pm 0.04$, $a_2 = 0.25 \pm 0.15$, and $m_0^\pi = 1.4 \pm 0.2$ GeV. In Fig. 9, we show the central values and the theoretical uncertainties of the NLO pQCD predictions for both form factors $f^+(q^2)$ and $f^0(q^2)$ of the $B \to \pi$ transition with the input hadron distribution amplitudes expressed in Eqs. (59) and (62), where the theoretical errors from different sources are added in quadrature. For the case of $q^2 = 0$ ($\eta = 1$), we find numerically that

$$f^+(0) = f^0(0) = 0.269^{+0.042}_{-0.035}(w_B)^{+0.028}_{-0.029}(a_2^\pi) \pm 0.020(m_0^\pi) = 0.269^{+0.054}_{-0.050}. \quad (78)$$

It is easy to see that the total theoretical error of the NLO pQCD prediction for $f^{+,0}(0)$ is about 20% of its central value, and it remains stable for the whole range of $0 \le q^2 \le 12$ GeV^2, as illustrated in Fig. 9.

In the previous numerical evaluations, we have used the most popular choices for both the b meson [35–39] and pion distribution amplitudes [4–6,40]: the B meson DAs as shown in Eq. (62) with the relation of $\phi_B = \phi_B^+ = \phi_B^-$ and the nonasymptotic pion DAs ϕ_π^A and $\phi_\pi^{P,T}$ as given in

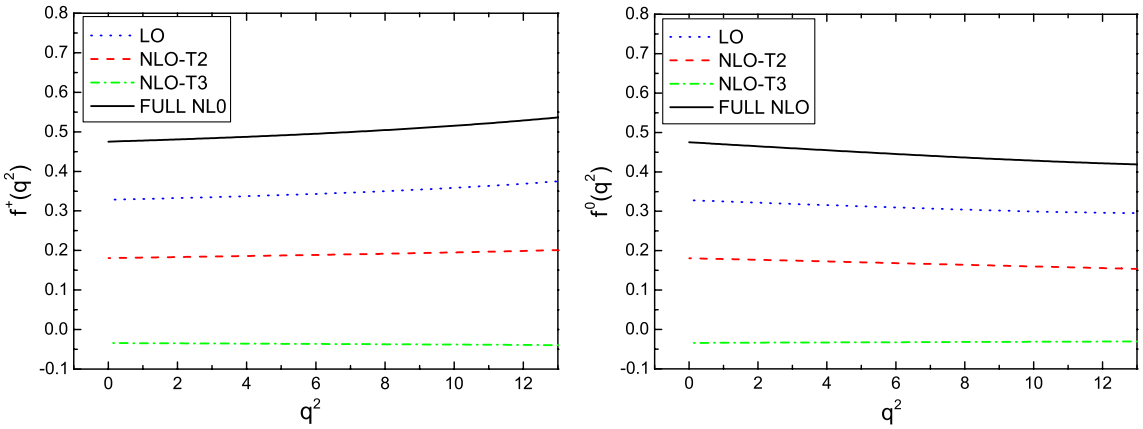

FIG. 11 (color online). The pQCD predictions for the form factors $f^+(q^2)$ and $f^0(q^2)$ for case C: the B meson DAs as given in Eq. (79) and the nonasymptotic pion DAs in Eq. (59) are used.

TABLE IV. The pQCD predictions for various contributions to $f_i^+(q^2)$ for $q^2 = (0, 5, 10)$ GeV^2 and their ratios $R_i(q^2) = f_i^+(q^2)/f_{\rm LO}^+(q^2)$ for case C.

Source	$f_i(0)$	$R_i(0)$	$f_i(5)$	$R_i(5)$	$f_i(10)$	$R_i(10)$
LO	0.328	100%	0.341	100%	0.358	100%
LO-T2	0.148	45.1%	0.146	42.8%	0.145	40.5%
NLO-T2	0.181	55.2%	0.188	55.1%	0.195	54.5%
LO-T3	0.180	54.9%	0.195	57.2%	0.213	59.5%
NLO-T3	−0.034	−10.4%	−0.036	−10.6%	−0.038	−10.6%
NLO	0.475	144.8%	0.493	144.6%	0.515	143.9%

Eq. (59). We denote this set of choices for the B meson and pion DAs as case A: $\phi_B(x,b)\oplus\phi_\pi^{A,P,T}$.

In Ref. [15], besides case A, the authors also considered other cases by using another form of the B meson DA inspired by the QCD sum rule [41] $\phi_B^{\rm II} = (\phi_B^+ + \phi_B^-)/2$ with different ϕ_B^+ and ϕ_B^-,

$$\phi_B^{(+)} = \frac{f_B}{2\sqrt{6}} x \left(\frac{m_B}{\omega_B}\right)^2 \cdot \exp\left[-\frac{x m_B}{\omega_B} - \frac{1}{2}(\omega_B b)^2\right],$$
$$\phi_B^{(-)} = \frac{f_B}{2\sqrt{6}} \left(\frac{m_B}{\omega_B}\right) \cdot \exp\left[-\frac{x m_B}{\omega_B} - \frac{1}{2}(\omega_B b)^2\right], \quad (79)$$

as well as the asymptotic pion DAs $\phi_\pi^{\rm asy}$,

$$\phi_\pi^A(x) = \frac{3 f_\pi}{\sqrt{6}} x(1-x), \qquad \phi_\pi^P(x) = \frac{f_\pi}{2\sqrt{6}},$$
$$\phi_\pi^T(x) = \frac{f_\pi}{2\sqrt{6}}(1-2x). \quad (80)$$

Following Ref. [15], here we will also make numerical calculations for three other possible choices of the B and pion meson DAs:

$$\text{case B} \quad \phi_B\oplus\phi_\pi^{\rm asy}, \quad \text{case C} \quad \phi_B^{\rm II}\oplus\phi_\pi, \quad \text{case D} \quad \phi_B^{\rm II}\oplus\phi_\pi^{\rm asy}. \quad (81)$$

We will compare the numerical results obtained for the different cases.

First, in Fig. 10 we show the q^2 dependence of the form factors for case B, i.e., the pQCD predictions for $f^+(q^2)$ and $f^0(q^2)$ obtained by using ϕ_B and $\phi_\pi^{\rm asy}$ as given in Eqs. (62) and (80), respectively. By this way, we can check the impact of the higher conformal-spin partial waves in the pion DAs, which partially arose from the nonzero pion mass correction. From the curves in Fig. 10, one can see that both form factors $f^+(q^2)$ and $f^0(q^2)$ are reduced by about 20% in the whole range of $0 < q^2 < 12$ Gev^2 when the additional Gegenbauer terms in the pion DAs are not included. Furthermore, in Table III we list the pQCD predictions for various contributions to $f^+(q^2)$ for $q^2 = (0, 5, 10)$ GeV^2 and their ratios $R_i(q^2) = f_i^+(q^2)/f_{\rm LO}^+(q^2)$ for case B. When compared with the numerical results for case A, as listed in Table II, we find that the NLO twist-3 contribution in case B plays a more important role than that for case A. For case B, the NLO twist-2 and NLO twist-3 contributions largely cancel each other, and the full NLO form factor then become a little smaller than the LO one.

In Fig. 11 and Table IV, we show the pQCD predictions for the form factors $f^+(q^2)$ and $f^0(q^2)$ and for their ratios $R_i(q^2) = f_i^+(q^2)/f_{\rm LO}^+(q^2)$ for case C, where the B meson DAs as given in Eq. (79) and the nonasymptotic pion DAs in Eq. (59) are used. The same input parameters as in case A are used here. For case C, we find that

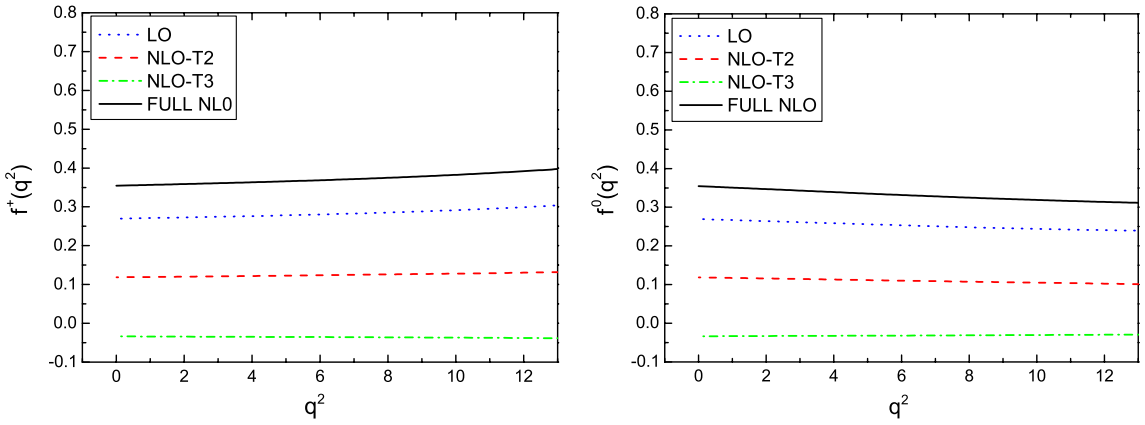

FIG. 12 (color online). The pQCD predictions for the form factors $f^+(q^2)$ and $f^0(q^2)$ for case D.

TABLE V. The pQCD predictions for various contributions to $f_i^+(q^2)$ for $q^2 = (0, 5, 10)$ GeV^2 and to their ratios $R_i(q^2) = f_i^+(q^2)/f_{\rm LO}^+(q^2)$ for case D.

Source	$f_i(0)$	$R_i(0)$	$f_i(5)$	$R_i(5)$	$f_i(10)$	$R_i(10)$
LO	0.270	100%	0.279	100%	0.290	100%
LO-T2	0.115	42.6%	0.114	40.9%	0.112	38.6%
NLO-T2	0.118	43.7%	0.123	44.1%	0.128	44.1%
LO-T3	0.155	57.4%	0.165	59.1%	0.178	61.4%
NLO-T3	−0.034	−12.6%	−0.035	−12.5%	−0.037	−12.8%
NLO	0.354	131.1%	0.367	131.5%	0.381	131.4%

(i) The LO contribution to the form factors $f^+(0)$ and $f^0(0)$ is 0.328 for case C, which is much larger than $f_i(0) = 0.251$ for case A, since the LO-T2 term for case C is 0.148, much larger than 0.086 for case A.
(ii) The net NLO contribution to the form factor $f_i(0)$ is about 0.15 for case C, much larger than 0.017 for case A, since the NLO-T2 term for case C is 0.181 instead of the small 0.061 for case A.
(iii) When we take all four parts into account, we find a large NLO pQCD prediction: $f_i(0) = 0.475$ for case C, which is much larger than $f_i(0) = 0.269$ for case A and also rather different from the popular values obtained by using the QCD sum rule.

In Fig. 12 and Table V, finally, we show the pQCD predictions for the form factors $f^+(q^2)$ and $f^0(q^2)$ and for their ratios $R_i(q^2) = f_i^+(q^2)/f_{\rm LO}^+(q^2)$ for case D, where the B meson DAs as given in Eq. (79) and the asymptotic pion DAs in Eq. (80) are used. The same input parameters as in case A are used here. For this case, both the LO-T2 and NLO-T2 terms become much larger than those for case A and lead to large LO and NLO pQCD predictions for $f_i(0)$. The NLO part here provides a 31% enhancement to the LO one.

V. SUMMARY

In this paper, by employing the k_T factorization theorem, we calculated the NLO twist-3 contribution to the form factors $f^+(q^2)$ and $f^0(q^2)$ of the $B \to \pi$ transition.

The UV divergences are renormalized into the coupling constants, decay constant, and quark fields. Both the soft and collinear divergences in the NLO QCD quark diagrams and in the NLO effective diagrams for meson wave functions are regulated by the off-shell momentum $k_{\rm iT}^2$ of the light quark. The heavy b quark is protected on shell to treat it as the standard effective heavy-quark field in the k_T factorization theorem, and then the soft gluon radiated by the b quark can be regularized by the gluon mass m_g. With the reasonable choice of $\xi_2^2 = m_B^2$, only the NLO corrections of the B meson function develop an additional double logarithm $\ln^2 r_1$, with $r_1 = \xi_1^2/m_B^2$, and then the resummation technique is implemented to minimize the scheme dependence from the different choice of ξ_1^2.

The cancellation of the IR divergences between the QCD quark diagrams and the effective diagrams for the meson wave functions at twist-3, in cooperation with the cancellation at the leading twist, verifies the validity of the k_T factorization for the $B \to \pi l^- \bar{\nu}_l$ semileptonic decays at the NLO level. The large double logarithm $\ln^2 x_1$ in the NLO hard kernel is resummed to result in the Sudakov factor, while the single logarithms and constant terms in the NLO hard kernel are all diminished by the choice of the scales μ and μ_f. We have demonstrated explicitly that the NLO corrections are under control.

From our numerical evaluations, we have generally found that the NLO pQCD predictions for the form factors $f^+(q^2)$ and $f^0(q^2)$ for case A agree well with those obtained by using the QCD sum rule. Based on our calculations, we find the following:

(i) For case A, the full LO and NLO pQCD predictions are $f_{\rm LO}^{+,0}(0) = 0.251$ and $f_{\rm NLO}^{+,0}(0) = 0.269$, which are consistent with those from the QCD sum rule.
(ii) There is a strong cancellation between the NLO twist-2 and NLO twist-3 contributions to the form factors $f^{+,0}(q^2)$ of the $B \to \pi$ transition. For the case of $f^+(0)$, for example, the NLO twist-2 contribution provides roughly a 24% enhancement to the full LO one, but the NLO twist-3 contribution makes a 17.5% decrease for the full LO result. The total NLO contribution results in a 7% enhancement to the LO pQCD prediction, which is small and stable for the whole range of $0 \le q^2 \le 12$ GeV^2.
(iii) For the other three cases, i.e., using different B meson and pion DAs in our numerical evaluations, the LO and NLO pQCD predictions will change accordingly. Generally speaking, the pQCD predictions for case C and case D are much larger than those obtained from the QCD sum rule.

ACKNOWLEDGMENTS

The authors would like to thank H. N. Li, Y. L. Shen, W. F. Wang, and X. Liu for valuable discussions. This work is supported by the National Natural Science Foundation of China under Grants No. 11235005, No. 11228512, and No. 11375208 and by the Project on Graduate Students Education and Innovation of Jiangsu Province under Grant No. CXZZ13-0391.

[1] J. Botts and G. Sterman, Nucl. Phys. **B325**, 62 (1989); H. N. Li and G. Sterman, Nucl. Phys. **B381**, 129 (1992); T. Huang and Q. X. Shen, Z. Phys. C **50**, 139 (1991); F. G. Cao, T. Huang, and C. W. Luo, Phys. Rev. D **52**, 5358 (1995).
[2] J. C. Collins and R. K. Ellis, Nucl. Phys. **B360**, 3 (1991).
[3] H. N. Li and H. L. Yu, Phys. Rev. Lett. **74**, 4388 (1995); **353**301 (1995); Phys. Rev. D **53**, 2480 (1996).
[4] G. P. Lepage and S. J. Brodsky, Phys. Lett. **87B**, 359 (1979).
[5] G. P. Lepage and S. J. Brodsky, Phys. Rev. D **22**, 2157 (1980).
[6] A. V. Efremov and A. V. Radyushkin, Phys. Lett. **94**, 245 (1980).
[7] G. Sterman, *An Introduction to Quantum Field Theory* (Cambridge University Press, Cambridge, England, 1993).
[8] M. Beneke and Th. Feldmann, Nucl. Phys. **B685**, 249 (2004).
[9] Y. Y. Keum, H. N. Li, and 'A. I. Sanda, Phys. Lett. **504**, 6 (2001); Phys. Rev. D **63**, 054008 (2001).
[10] C. D. Lü, K. Ukai, and M. Z. Yang, Phys. Rev. D **63**, 074009 (2001); C. D. Lü and M. Z. Yang, Eur. Phys. J. C **28**, 515 (2003); H. Kawamura, J. Kodaira, C. F. Qiao, and K. Tanaka, Phys. Lett. **523**, 111 (2001).
[11] J. P. Ralston and B. Pire, Phys. Rev. Lett. **65**, 2343 (1990).
[12] H. N. Li, Prog. Part. Nucl. Phys. **51**, 85 (2003).
[13] S. Nandi and H. N. Li, Phys. Rev. D **76**, 034008 (2007).
[14] H. N. Li, Y. L. Shen, Y. M. Wang, and H. Zou, Phys. Rev. D **83**, 054029 (2011).
[15] H. N. Li, Y. L. Shen, and Y. M. Wang, Phys. Rev. D **85**, 074004 (2012).
[16] H. N. Li, Y. L. Shen, and Y. M. Wang, J. High Energy Phys. 01 (2014) 004.
[17] S. Cheng, Y. Y. Fan, and Z. J. Xiao, Phys. Rev. D **89**, 054015 (2014).
[18] H. N. Li, Phys. Rev. D **66**, 094010 (2002).
[19] H. N. Li, Phys. Lett. **555**, 197 (2003).
[20] M. Beneke and Th. Feldmann, Nucl. Phys. **B592**, 3 (2000).
[21] T. Kurimoto, H. N. Li, and A. I. Sanda, Phys. Rev. D **65**, 014007 (2001).
[22] C. D. Lü and M. Z. Yang, Eur. Phys. J. C **23**, 275 (2002).
[23] W. Siegel, Phys. Lett. **84**, 193 (1979).
[24] H. N. Li and H. S. Liao, Phys. Rev. D **70**, 074030 (2004).
[25] H. N. Li, Phys. Rev. D **64**, 014019 (2001).
[26] M. Nagashima and H. N. Li, Eur. Phys. J. C **40**, 395 (2005).
[27] X. Ji and F. Yuan, Phys. Lett. **543**, 66 (2002).
[28] J. C. Collins, Acta Phys. Pol. B **34**, 3103 (2003).
[29] J. P. Ma and Q. Wang, J. High Energy Phys. 01 (2006) 067; Phys. Lett. **642**, 232 (2006).
[30] M. Nagashima and H. N. Li, Phys. Rev. D **67**, 034001 (2003).
[31] V. M. Braun and I. E. Filyanov, Z. Phys. C **48**, 239 (1990).
[32] P. Ball, J. High Energy Phys. 01 (1999) 010.
[33] P. Ball and R. Zwicky, Phys. Rev. D **71**, 014015 (2005).
[34] P. Ball, V. M. Braun, and A. Lenz, J. High Energy Phys. 05 (2006) 004; P. Ball, V. M. Braun, Y. Koike, and K. Tanaka, Nucl. Phys. **B529**, 323 (1998); P. Ball, J. High Energy Phys. 09 (1998) 005.
[35] B. O. Lange and M. Neubert, Phys. Rev. Lett. **91**, 102001 (2003).
[36] V. M. Braun, D. Yu. Ivanov, and G. P. Korchemsky, Phys. Rev. D **69**, 034014 (2004).
[37] G. Bell and T. Feldmann, J. High Energy Phys. 04 (2008) 061.
[38] S. Descotes-Genon and N. Offen, J. High Energy Phys. 05 (2009) 091.
[39] M. Knoedlseder and N. Offen, J. High Energy Phys. 10 (2011) 069.
[40] G. P. Lepage and S. J. Brodsky, Phys. Rev. Lett. **43**, 1625(E) (1979).
[41] A. G. Grozin and M. Neubert, Phys. Rev. D **55**, 272 (1997).